The role of the N-terminal domain of human apurinic/apyrimidinic endonuclease 1, APE1, in DNA glycosylase stimulation

Olga Kladova, Milena Bazlekowa-Karaban, Sonia Baconnais, Olivier Pietrement, Alexander Ishchenko, Bakhyt Matkarimov, Olga A Fedorova, Eric Le Cam, Barbara Tudek, Nikita Kuznetsov, et al.

The role of the N-terminal domain of human apurinic/apyrimidinic endonuclease 1, APE1, in DNA glycosylase stimulation

Olga Kladova[a], Milena Bazlekowa-Karaban[b,c], Sonia Baconnais[d], Olivier Pietrement[d], Alexander A. Ishchenko[c], Bakhyt T. Matkarimov[e], Olga S. Fedorova[a], Eric Le Cam[d], Barbara Tudek[b,f], Nikita A. Kuznetsov[a,] and Murat Saparbaev[c,]**

[a]*SB RAS Institute of Chemical Biology and Fundamental Medicine, Novosibirsk 630090, Russia.*

[b]*Institute of Biochemistry and Biophysics, Polish Academy of Sciences, 02-106 Warsaw, Poland.*

[c]*Groupe «Réparation de l'ADN», Equipe Labellisée par la Ligue Nationale contre le Cancer, CNRS UMR8200, Université Paris-Sud, Gustave Roussy Cancer Campus, F-94805 Villejuif Cedex, France.*

[d]*CNRS UMR8126, Université Paris-Sud, Gustave Roussy Cancer Campus, F-94805 Villejuif Cedex, France.*

[e]*National laboratory Astana, Nazarbayev University, Astana 010000, Kazakhstan.*

[f]*Institute of Genetics and Biotechnology, University of Warsaw, Warsaw, Poland.*

**Corresponding authors. M.S. and N.A.K.: phone: +33 1-42115404; Email: murat.saparbaev@gustaveroussy.fr and phone: +7 (383) 363-5174. E-mail address: nikita.kuznetsov@niboch.nsc.ru.*

Keywords: oxidative DNA damage; apurinic/apyrimidinic site; base excision repair; redox function; DNA glycosylase; AP lyase; AP endonuclease.

ABBREVIATIONS

ROS, reactive oxygen species; AP, apurinic/apyrimidinic site; THF, 3-hydroxy-2-hydroxymethyltetrahydrofuran or tetrahydrofuran; Ura, uracil; dU, 2′-deoxyuridine; αdA, α-anomeric 2′-deoxyadenosine; Hx, hypoxanthine; 8oxoG, 7,8-dihydro-8-oxoguanine; BER, base excision repair; NIR, nucleotide incision repair; APE1 (a.k.a. APEX1, HAP-1, or Ref-1), human major AP endonuclease 1; OGG1, human 8-oxoguanine-DNA glycosylase; MBD4 (a.k.a. MED1), human methyl-binding domain protein 4; MBD4^{cat}, catalytic domain of MBD4; ANPG (a.k.a. Aag or MPG), human alkyl-*N*-purine-DNA glycosylase; ANPG^{cat}, catalytic domain of ANPG; TDG, human mismatch-specific thymine-DNA glycosylase; Nfo, *Escherichia coli* endonuclease IV; ARP, *Arabidopsis thaliana* AP endonuclease.

ABSTRACT

The base excision repair (BER) pathway consists of sequential action of DNA glycosylase and apurinic/apyrimidinic (AP) endonuclease necessary to remove a damaged base and generate a single-strand break in duplex DNA. Human multifunctional AP endonuclease 1 (APE1, a.k.a. APEX1, HAP-1, or Ref-1) plays essential roles in BER by acting downstream of DNA glycosylases to incise a DNA duplex at AP sites and remove 3′-blocking sugar moieties at DNA strand breaks. Human 8-oxoguanine-DNA glycosylase (OGG1), methyl-CpG-binding domain 4 (MBD4, a.k.a. MED1), and alkyl-*N*-purine-DNA glycosylase (ANPG, a.k.a. Aag or MPG) excise a variety of damaged bases from DNA. Here we demonstrated that the redox-deficient truncated APE1 protein lacking the first N-terminal 61 amino acid residues (APE1-NΔ61) cannot stimulate DNA glycosylase activities of OGG1, MBD4, and ANPG on duplex DNA substrates. Electron microscopy imaging of APE1–DNA complexes revealed oligomerization of APE1 along the DNA duplex and APE1-mediated DNA bridging followed by DNA aggregation. APE1 polymerizes on both undamaged and damaged DNA in cooperative mode. Association of APE1 with undamaged DNA may enable scanning for damage; however, this event reduces effective concentration of the enzyme and subsequently decreases APE1-catalyzed cleavage rates on long DNA substrates. We propose that APE1 oligomers on DNA induce helix distortions thereby enhancing molecular recognition of DNA lesions by DNA glycosylases *via* a conformational proofreading/selection mechanism. Thus, APE1-mediated structural deformations of the DNA helix stabilize the enzyme–substrate complex and promote dissociation of human DNA glycosylases from the AP site with a subsequent increase in their turnover rate.

Significance Statement

The major human apurinic/apyrimidinic (AP) endonuclease, APE1, stimulates DNA glycosylases by increasing their turnover rate on duplex DNA substrates. At present, the mechanism of the stimulation remains unclear. We report that the redox domain of APE1 is necessary for the active mode of stimulation of DNA glycosylases. Electron microscopy revealed that full-length APE1 oligomerizes on DNA possibly via cooperative binding to DNA. Consequently, APE1 shows DNA length dependence with preferential repair of short DNA duplexes. We propose that APE1-catalyzed oligomerization along DNA induces helix distortions, which in turn enable conformational selection and stimulation of DNA glycosylases. This new biochemical property of APE1 sheds light on the mechanism of redox function and its role in DNA repair.

1. Introduction

DNA repair is essential for cell survival and for tissue homeostasis given that cellular DNA is constantly challenged by various endogenous and exogenous genotoxic factors that generate DNA damage: structural and chemical modifications of a primary DNA sequence. Various organisms have evolved multiple DNA repair systems to deal with these insults. Nonbulky base damage is specifically recognized among the vast majority of regular bases by DNA glycosylases and apurinic/apyrimidinic (AP) endonucleases in the base excision repair (BER) and nucleotide incision repair (NIR) pathways, respectively [1-4]. In the BER pathway, a DNA glycosylase hydrolyses the *N*-glycosidic bond between the damaged base and sugar, leaving either an apurinic/apyrimidinic (AP) site or a single-stranded DNA break. Based on the mechanism of action, DNA glycosylases are classified into mono- and bifunctional. Monofunctional DNA glycosylases such as human mismatch-specific thymine-DNA glycosylase (TDG), methyl-CpG-binding domain 4 (MBD4, a.k.a. MED1), and alkyl-*N*-purine-DNA glycosylase (ANPG, a.k.a. Aag or MPG) cleave the *N*-glycosidic bond, releasing the modified base and generating an AP site [5-7]. Bifunctional DNA glycosylases such as human 8-oxoguanine-DNA glycosylase 1 (OGG1) and endonuclease VIII-like glycosylases (NEIL1-3) not only cleave the *N*-glycosidic bond but also exert an associated AP lyase activity that eliminates the 3′ phosphate (β-elimination) or 3′ and 5′ phosphates (β,δ-elimination) of the resulting AP site either in a concerted or in a nonconcerted manner [8-9]. It should be noted that mammalian bifunctional DNA glycosylases such as NEIL1 and NEIL2 excise the modified base and cleave the resulting AP site in DNA via β/δ-elimination in a highly concerted manner [10-11]. In contrast, other bifunctional DNA glycosylases such as OGG1 and NEIL3 manifest nonconcerted action, with base excision being more efficient than AP site cleavage activity [8, 12]. β-Elimination produces a nick flanked by a 3′-terminal α,β-

unsaturated aldehyde and a 5′-terminal phosphate, whereas β,δ-elimination yields a single-nucleoside gap flanked by two phosphates [13-14]. At a subsequent step, the 3′-terminal phosphoaldehyde and phosphate are removed by an AP endonuclease and polynucleotide kinase (PNK), respectively, allowing DNA polymerase to fill the gap before DNA ligase seals the resulting DNA nick [15-16].

BER, initiated by multiple DNA glycosylases, is the main pathway for removal of the majority of nonbulky DNA lesions [17-18]; however, a certain type of lesions—such as the α-anomers of 2′-deoxynucleosides (αdN)—is repaired by AP endonucleases in the NIR pathway, not by DNA glycosylases [19-21]. Human major apurinic/apyrimidinic (AP) endonuclease 1 (APE1, a.k.a. APEX1, HAP-1, or Ref-1) plays essential roles in both pathways. In BER, it acts downstream of DNA glycosylases by incising a DNA duplex at AP sites and removing 3′-blocking sugar phosphate moieties. Alternatively, in NIR, APE1 makes an incision 5′ to a damaged base and generates a single-strand break with a 5′-dangling modified nucleotide and a 3′-hydroxyl group [21-22]. Human APE1 is a ubiquitous 36-kDa multifunctional protein that performs essential functions in DNA repair, transcription, RNA biogenesis, and cell proliferation [23-24]. Moreover, DNA substrate specificity of APE1 is modulated by concentrations of divalent cations, pH, and ionic strength in an apparently allosteric manner [21]. At low concentrations of Mg^{2+} (≤1 mM) and acidic or neutral pH (≤7), APE1 binds strongly to both the DNA substrate and the reaction product and exerts NIR endonuclease activity. By contrast, at high concentrations of Mg^{2+} (≤5 mM) and neutral or alkaline pH (≤8), APE1 shows high AP site cleavage activity mainly due to a dramatic increase in the enzyme turnover rate. Changes in intracellular Mg^{2+} concentration can induce conformational changes in the APE1 protein [21, 25]. Due to dynamic conformational changes, APE1 can recognize diverse types of DNA base lesions including αdN, oxidized pyrimidines [21, 26], formamidopyrimidines [27], exocyclic DNA bases, thymine glycol, uracil [28-29], and bulky

lesions such as benzene-derived DNA adducts [30] and a UV-induced 6-4 photoproduct [31]. Furthermore, the chemical structures of these DNA lesions have very little in common, implying that contrary to DNA glycosylases, APE1 tends to recognize damage-induced structural distortions of the DNA helix and not a modified base itself.

DNA glycosylase stimulation by APE1. Tight binding to an abasic site in duplex DNA appears to be a common feature of DNA glycosylases [32]. Kinetic characterization of human monofunctional TDG, MBD4, ANPG, and bifunctional OGG1 DNA glycosylases has revealed that their product release is rate limiting during the steady-state phase of the reaction [33-35]. Numerous studies have revealed that APE1 promotes dissociation of the DNA glycosylase–product complex, and this situation in turn increases multiple turnover rates of TDG, ANPG, and OGG1 [36-39]. APE1 enhances the product release rate constant but not the rate constant of base excision by the DNA glycosylases. Notably, the APE1 protein is highly abundant, and its concentration is estimated at 1–7 million molecules per cell [40]. Thus, the intracellular concentration of APE1 is higher than that of DNA polymerase β (50,000 per cell) [41] and human DNA glycosylases (UNG2, SMUG1, and TDG) [42]. Two mechanisms were proposed to explain the stimulation of DNA glycosylases by APE1: a passive mechanism, when an AP endonuclease depletes (cleaves) a free AP site to prevent its rebinding with the DNA glycosylase during the reaction [33, 39, 43-44] and an active mechanism, which consists of direct displacement of DNA glycosylase from the AP site either via specific protein–protein interactions [36] or through distortion of the duplex DNA structure to disrupt the DNA glycosylase–AP site DNA complex [45]. Several lines of evidence suggest that APE1 actively displaces DNA glycosylases from the AP site in duplex DNA. Indeed, the displacement of DNA glycosylases by APE1 does not require AP site cleavage activity because robust stimulation is observed in the absence of Mg^{2+} (essential for this catalysis) [46], and when the catalytically inactive APE1-D210N mutant is used [43].

Furthermore, APE1 can increase the turnover of TDG and ANPG to 40 and 100 times the observed rates of DNA glycosylase's dissociation from DNA of the AP site, respectively, indicating that APE1 follows the active mechanism of the stimulation [46-47]. It remains puzzling how the activities of various DNA glycosylases are stimulated by APE1 because these repair enzymes belong to different structural families without a common structural motif that could be involved in the specific protein–protein interaction.

APE1 was independently discovered as an abasic site-specific endonuclease homologous to the *E. coli* Xth protein [48-49] and as a redox factor (Ref-1) that regulates the DNA-binding domain of Fos-Jun, Jun-Jun, AP-1 proteins, and several other transcription factors [50]. Within cells, reactive oxygen species (ROS) can serve as signaling molecules because an increase in $O_2\bullet^-$ and H_2O_2 concentrations activates various signaling pathways through a specific gene expression pattern. Gene expression is controlled by transcription factors (sequence-specific DNA-binding proteins), which are often regulated by post-translational modifications. Particularly, the DNA-binding activity of mammalian transcription factor AP-1 (Fos-Jun heterodimer protein) is subject to reduction-oxidation (redox) regulation. This regulation is implemented via post-translational modification of a conserved cysteine residue in the DNA-binding domains of Fos and Jun [51]. Notably, oxidation of the cysteines by ROS strongly inhibits the DNA-binding activity of AP-1, and this inhibition can be reversed by reduction of the cysteines by thiol compounds or by the APE1 (Ref-1) protein [50]. It was proposed that APE1 activates these transcription factors via a redox mechanism by mediating the reduction of a cysteine (Cys) residue in its DNA-binding domain. The APE1 protein can be subdivided into two functionally distinct and partially overlapping regions: the N-terminal domain (amino acid residues 1–127) possessing the redox activity and the C-terminal domain (amino acid residues 61–318), which is responsible for the AP site cleavage activity [52-53]. Suppression of APE1 results in embryonic death in mice

[54], inhibits human cell proliferation [55], induces apoptosis in mouse embryonic fibroblasts [56], and causes telomere shortening [57]. At present, the role of non-DNA repair functions of APE1 in embryonic development and cell proliferation remain unclear.

It has been demonstrated that deletion of the first N-terminal 61 amino acids residues in APE1 (APE1-NΔ61) decreases redox activity but does not influence AP site cleavage activity [53]. Later, a study by our laboratory revealed that the truncated APE1-NΔ61 protein shows a dramatic decrease in the NIR activity, pointing to a common mechanism of action for the APE1-catalyzed NIR and redox functions [21]. These observations prompted us to investigate the role of the first 61 N-terminal amino acid residues of APE1 in the stimulation of human DNA glycosylases. Here we demonstrate that in contrast to wild-type (WT) APE1, the APE1-NΔ61 mutant cannot stimulate the multiple turnover of DNA glycosylases. Electron microscopy (EM) indicated that APE1 can oligomerize onto a DNA fragment, introducing helix deformation to scan undamaged DNA in search of abasic sites. In contrast, atomic force microscopy (AFM) revealed that APE1 oligomerization induces a kink in the DNA backbone to detect an abasic site. The evolutionary conservation, structural basis, and potential biological importance of the reported new biochemical property of APE1 are then discussed.

2. Materials and methods

2.1. Oligonucleotides and proteins

Sequences of all the oligodeoxyribonucleotides used in this work are presented in Table 1. All the oligonucleotides were purchased from Eurogentec (Seraing, Belgium) including those containing uracil (U), hypoxanthine (Hx), tetrahydrofuran (THF), αdA, or 8-oxoguanine (8oxoG). The complementary oligonucleotides contained dA, dG, dC, or T opposite the lesion. Prior to enzymatic assays, oligonucleotides were either 3′-end-labeled by terminal deoxynucleotidyl transferase (New England Biolabs, France) in the presence of [α-^{32}P]3′-

dATP (cordycepin 5′-triphosphate, 5,000 Ci/mmol) or 5′-end-labeled by means of T4 polynucleotide kinase (New England Biolabs) in the presence of [γ-^{32}P]ATP (3,000 Ci/mmol, PerkinElmer – Life Science Research, Courtaboeuf, France), as recommended by the manufacturers. The radioactively labeled oligonucleotides were desalted on a Sephadex G-25 column equilibrated with water and then annealed to a desired complementary strand for 3 min at 65 °C in a buffer consisting of 20 mM HEPES-KOH (pH 7.6) and 50 mM KCl and then were slowly cooled to room temperature.

Purified OGG1, ANPG^{cat}, MBD4^{cat}, *E. coli* endonuclease IV (Nfo) and *Arabidopsis thaliana* major AP endonuclease (ARP) were from the laboratory stock. Human alkyl-*N*-purine-DNA glycosylase, ANPG^{cat}, with the first 73 amino acid residues deleted from the N terminus was purified as described elsewhere [58]. The purification of human 8-oxoguanine-DNA glycosylase OGG1 was carried out as described previously [59]. Human major AP endonuclease APE1 and its mutant versions (APE1-NΔ61 and APE1-D210N) were expressed and purified in their native form without tags or other modifications as described previously [26]. The catalytic domain of methyl-CpG-binding domain protein 4, MBD4^{cat} (residues 426–580) was purified as described elsewhere [60]. Nfo and ARP were purified as described elsewhere [61-62].

2.2. DNA repair assays

The standard reaction mixture (20 μL) for DNA glycosylases without divalent cations contained 50 nM ^{32}P-labeled oligonucleotide duplex, 15 nM OGG1 (or 20 nM MBD4^{cat}, 15 nM ANPG^{cat}) and 50–2000 nM APE1-WT or its mutated versions (NΔ61, NΔ31, NΔ35, or D210N) in a buffer (BER-EDTA conditions) consisting of 20 mM Tris-HCl pH 8.1, 100 mM NaCl, 1 mM EDTA, 1 mM DTT, 0.1 mg/mL BSA, and incubated for 30 min at 37°C, unless stated otherwise. All the reactions were stopped by addition of 10 μL of a stop solution

consisting of 0.5% SDS and 20 mM EDTA. Then, the reaction mixture was exposed to light piperidine treatment [10% (v/v) piperidine at 37°C for 30 min] to cleave the AP sites left after the excision of a damaged base. After incubation, the solution was neutralized with 4.5 μL of 2 M HCl.

The standard AP endonuclease assay was conducted at a high Mg^{2+} concentration (≥5 mM) and pH 7.6 (BER conditions): the reaction mixture (20 μL) consisted of 10 nM ^{32}P-labeled THF•T duplex oligonucleotide, 5 mM $MgCl_2$, 100 mM KCl, 20 mM Hepes-KOH pH 7.6, 0.1 mg/mL BSA and 0.1 nM enzyme, unless specified otherwise. The standard NIR assay was performed at a low Mg^{2+} concentration (≤1 mM) and acidic or neutral pH (≤7; NIR conditions): the reaction mixture (20 μL) consisted of 10 nM ^{32}P-labeled αdA•T duplex oligonucleotide, 0.5 mM $MgCl_2$, 25 mM KCl, 20 mM HEPES-KOH pH 6.8, 0.1 mg/mL BSA, and either 2 nM APE1 or 0.1 nM Nfo, unless specified otherwise. All the reactions were stopped by addition of 10 μL of the stop solution.

After the reactions, all the samples were desalted on hand-made spin-down columns packed with Sephadex G25 (Amersham Biosciences) equilibrated with 7.5 M urea. The purified reaction products were separated by electrophoresis in a denaturing 20% (w/v) polyacrylamide gel (7.5 M urea, 0.5× Tris-borate-EDTA buffer, 42°C). The gels were used for exposure of a Storage Fuji FLA-3000 Phosphor Screen, which was then scanned using Typhoon FLA 9500, and the digital images were obtained and quantified in the FUJI Image Gauge v.3.12 software. At least three independent experiments were conducted for all kinetic measurements.

2.3. Stopped-flow fluorescence measurements

The pre-steady-state kinetics were studied by the stopped-flow technique with detection of a fluorescence signal generated during fluorescence resonance energy transfer

(FRET) between a fluorophore and quencher as previously described [63-64] on an SX.18MV stopped-flow spectrometer (Applied Photophysics). A 6-carboxyfluorescein (FAM) residue and black hole quencher (BHQ1) were present in the FRET substrates (Table 1); the wavelength λ_{ex} = 494 nm was used for excitation, and emission was analyzed at λ_{em} > 515 nm (Schott filter OG-515). The dead time of the instrument was 1.4 ms. Concentrations of DNA glycosylases and DNA substrates were 1 µM, and concentrations of APE1 proteins were 0.5–5.0 µM. The concentrations of reactants reported are those in the reaction chamber after mixing. All stopped-flow fluorescence measurements were carried out at 37°C in BER-EDTA reaction buffer [20 mM Tris-HCl (pH 8.1), 100 mM KCl, 1 mM EDTA, 1 mM dithiothreitol, and 7% glycerol (v/v)]. Typically, each trace shown is an average of three or more independent experiments. Experimental error was less than 5%. Each phase on the kinetic curve allowed us to calculate two parameters: the amplitude of this phase and the observed rate constant. The process should be finished within recorded time range to correct calculation of the parameters.

Data obtained in the fluorescence stopped-flow kinetic assays were fitted by means of the following exponential Eq. 1, using the Origin software (Originlab Corp.):

$$F = F_0 + F_1 \exp(-k_1 t) + F_2 \exp(-k_2 t) \qquad (1)$$

where F is the observed FAM fluorescence intensity, F_0 is background fluorescence, F_i is a fluorescence parameter, and k_i denotes the observed rate constant.

2.4. Electron microscopy

A 1440-bp dsDNA fragment was amplified by PCR from the pBR322 plasmid (NEB, France) as described elsewhere [65]. For molecular imaging experiments, all DNA molecules

were purified on a Mini Q anion exchange column using a SMART chromatography system (GE Healthcare). The purified DNA was precipitated with ethanol and resuspended in TE buffer (10 mM Tris-HCl pH 7.5, 1 mM EDTA). Transmission electron microscopy (TEM) samples were prepared by positive staining as previously described [65]. All nucleoprotein complexes were formed by incubation at 4°C for 10 min in binding buffer (10 mM Tris-HCl pH 8, 50 mM NaCl) containing 5 nM 1440-bp DNA fragment in the presence of 100 nM APE1-WT or APE1-NΔ61 protein, which corresponds to a final protein/nucleotides ratio of 1/72. Immediately before spreading on the microscopy grid, the DNA–protein reaction was diluted 20-fold in binding buffer. Five microliters of this dilution was deposited onto a 600-mesh copper grid coated with a thin carbon film, preactivated by glow-discharge in the presence of pentylamine (Sigma-Aldrich, France). The grids were washed with aqueous 2% (w/v) uranyl acetate (Merck, France) and then dried with ashless filter paper (VWR, France). TEM examination was carried out under a Zeiss 912AB transmission electron microscope in filtered crystallographic dark-field mode. Electron micrographs were captured using a Tengra high-resolution CCD camera and iTEM software (Olympus, Soft Imaging Solutions).

2.5. AFM analysis of the APE1–DNA complexes

A short DNA fragment containing a single abasic site in the middle of the sequence was prepared. For this purpose, a 20-bp double-stranded oligonucleotide containing a single abasic site at its center was ligated using T4 DNA ligase with two 95-bp fragments on both sides of the site to generate a 210-bp fragment. The ligated DNA fragments were purified by chromatography on a Mono Q ion exchange column by means of a Smart chromatography system (GE Healthcare). APE1–DNA complexes were incubated in binding buffer (100 mM NaCl, 5 mM $MgCl_2$, 20 mM Tris-HCl pH 7.5) at 20°C for 10 min. A 5-µL droplet of the

APE1 (100 nM) and DNA solution at 2 µg/mL (3 µM nucleotide and 14 nM AP site) was deposited onto the surface of freshly cleaved mica (muscovite) for 1 min. Then, the surface was rinsed with a 0.002% diluted uranyl acetate solution to stabilize the complexes for AFM imaging in air [66]. The sample was then rapidly rinsed with Milli-Q water (EMD Millipore, Bedford, MA) to obtain a clean surface after drying with filter paper. AFM imaging was carried out in intermittent contact mode on a Multimode system (Bruker) operating with a Nanoscope IIA controller (Bruker). We used silicon AC200TS cantilevers (Olympus) with resonance frequencies of ~150 kHz. All images were acquired at a scan frequency of 1 Hz and resolution 512 × 512 pixels. The images were analyzed in the Nanoscope IIIA software and a third-order polynomial function was employed to remove the background.

3. Results

3.1. The role of the redox domain of APE1 in stimulation of 8oxoG-DNA glycosylase activity of OGG1

To test whether the redox domain of APE1 is involved in DNA glycosylase stimulation, we measured 8oxoG-DNA glycosylase activity of OGG1 in the presence of APE1-WT or truncated mutant APE1-NΔ61. To this end, 50 nM 5′-^{32}P-labeled 40mer 8oxoG•C duplex was incubated with 15 nM OGG1 protein in BER-EDTA buffer in the presence of various concentrations of APE1 proteins. It should be noted that we used a reaction buffer containing EDTA and no divalent cations to avoid the passive mode of stimulation of DNA glycosylases by APE1. Recently, we demonstrated that Mg^{2+} ions have no effect on the initial formation of the APE1–DNA complex; however, formation of the catalytic complex as well as the rate of catalytic reaction strongly depend on the concentration of Mg^{2+} [67]. After the reaction, to reveal the presence of uncleaved AP sites, the samples were mildly treated with piperidine (10% [v/v] piperidine at 37 °C for 30 min) and then analyzed by polyacrylamide gel electrophoresis (PAGE) in a 20% denaturing gel. As shown in Fig. 1, incubation of 8oxoG•C with OGG1 led to formation of a small amount of the 19mer cleavage fragment indicating excision of 8oxoG base at position 20 (Fig. 1*A*, lanes 2 and 9). It should be noted that OGG1 has a weak AP lyase activity, and after excision of 8oxoG, the enzyme remains associated with an intact AP site for a relatively long time [8]. Vidal and colleagues showed that APE1 stimulates only the hOGG1-catalyzed base excision but not AP site cleavage, thus accentuating the uncoupling of OGG1 glycosylase and AP lyase activities [43]. Here, the piperidine treatment efficiently incised an AP site in DNA via β-elimination and generated a 5′-^{32}P-labeled cleavage fragment containing a 3′-phospho α,β-unsaturated aldehyde. Addition of greater amounts of the APE1-WT protein resulted in a dramatic increase in 8oxoG•C cleavage and appearance of an additional faster-migrating cleavage

product (lanes 3–7). These observations confirm the findings of Vidal and colleagues and indicate that APE1 increases AP site formation via stimulation of the turnover of OGG1-catalyzed DNA glycosylase activity on the 8oxoG•C duplex. Formation of a faster-migrating cleavage product indicates that at high protein concentrations, APE1 can cleave AP sites even in the presence of 1 mM EDTA and generate a 5′-^{32}P-labeled cleavage fragment containing a 3′-hydroxyl group. In contrast to APE1-WT, addition of greater concentrations of the truncated mutant APE1-NΔ61 into the reaction did not result in effective stimulation of OGG1 on the 8oxoG•C duplex (lanes 10–14). This result was quite surprising because the APE1-NΔ61 mutant, just as the wild-type enzyme, has a very efficient AP site cleavage activity [53, 68]. The inability of the truncated APE1 protein to stimulate OGG1 implies the involvement of N-terminal amino acids in the active displacement of DNA glycosylase from the AP site in DNA.

Next, we determined whether catalytically inactive APE1-D210N mutant and truncated APE1 variants lacking the first N-terminal 31 or 35 amino acid residues (APE1-NΔ31 and APE1-NΔ35, respectively) would stimulate OGG1 on the 8oxoG•C duplex. Previously, we have shown that truncated APE1-NΔ31 and APE1-NΔ35 mutants perform the NIR function [26]. Of note, the APE1-D210N, APE1-NΔ31, and APE1-NΔ35 mutants were still able to increase the turnover rate of OGG1 to the same extent as the APE1-WT protein did (Fig. 1*B* and *SI Appendix*, Fig. S1). As expected, incubation of the APE1-D210N mutant with OGG1 and 8oxoG•C duplex did not generate a faster-migrating 19mer cleavage product (Fig. S1). This result indicates that the 19mer cleavage fragment observed during stimulation of OGG1 by APE1 is a product of the hydrolytic cleavage of the abasic site by the human AP endonuclease. To further substantiate the involvement of the redox domain of APE1 in DNA glycosylase stimulation, we analyzed bacterial and plant AP endonucleases: *E. coli* endonuclease IV (Nfo) and *Arabidopsis thaliana* AP endonuclease (ARP) for their ability to

stimulate OGG1 on the 8oxoG•C duplex. The results showed that at any given concentration, the Nfo protein moderately stimulated OGG1 and could cleave AP site DNA in the absence of Mg^{2+} (*SI Appendix*, Fig. S2). This result suggests that bacterial AP endonuclease acts in a passive manner by cleaving AP sites that are released after spontaneous dissociation of DNA glycosylase. No DNA glycosylase stimulation was observed in the presence of the plant ARP protein, suggesting that AP endonucleases from other species, where a native redox domain is absent, cannot stimulate active dissociation of the OGG1–AP site DNA complex.

3.2. Conformational transitions in a fluorophore-labeled FRET-8oxoG•C duplex in the presence of OGG1 and APE1

To elucidate the nature of OGG1 stimulation by APE1, we registered the processes of complex formation between OGG1 and the FRET-8oxoG•C duplex and subsequent N-glycosidic bond hydrolysis (DNA glycosylase activity) and DNA cleavage (AP lyase activity) in a pre-steady-state stopped-flow assay of the FRET signal (Fig. 2*A*). Interaction of OGG1 with FRET-8oxoG•C led to a decrease in the FRET signal in the initial part of the kinetic curve up to 20 s. The initial drop-off in the FRET signal indicates stabilization of the DNA duplex ends that causes a slight decrease and fixation of the distance within the FRET pair of dyes in the enzyme–DNA complex. Structural and kinetic data suggested that the observed decrease in the FRET signal characterizes a conformational change (of the enzyme and DNA) leading to formation of a tight complex and the catalytically competent state [69-71]. These data are in agreement with our previous kinetic results showing that the catalytic complex is formed during the initial 50–100 s of the interaction [72-73].

The solutions of OGG1 and of the FRET-8oxoG•C substrate were mixed in the presence of various concentrations of APE1-WT, APE1-NΔ61, or Nfo (Fig. 2*A* and *SI Appendix*, Fig. S3).

The hydrolysis of the N-glycosidic bond of the damaged nucleotide resulted in formation of an abasic site product. OGG1 is a bifunctional enzyme, but the AP lyase activity of OGG1 is much weaker than its DNA glycosylase activity [70-71, 74]. Formation of the AP site and subsequent slow disruption of the OGG1 complex with an abasic product enhance the mobility of duplex chains and increase the distance between FRET-dyes, which increases the FRET signal in the 50–1000 s interval (Fig. 2*A*). We examined the effect of APE1-WT on OGG1 action (DNA binding and product release) by analysis of kinetic traces obtained at varied concentrations of APE1-WT (*SI Appendix*, Fig. S3*A*). Preincubation of OGG1 with APE1-WT for 15 min and subsequent mixing with the FRET-8oxoG•C substrate led to a dramatic increase in the amplitude of the FRET signal as compared with the kinetic trace without APE1-WT. It should be noted that mixing only APE1-WT with the FRET-8oxoG•C duplex did not yield changes in the FRET signal (Fig. 2*A*). Kinetic traces obtained for each concentration of APE1-WT were processed according to Eq. 1, and values of the observed rate constants of the complex formation (k_1) and product release followed by the glycosylase reaction (k_2) were calculated. We found that the observed rate constant k_1 (*SI Appendix*, Fig. S3*B*) does not depend on the concentration of APE1-WT, indicating that the AP endonuclease does not affect the rate of complex formation between OGG1 and DNA containing 8oxoG. At the same time, an increase in the amplitude of the FRET signal in the presence of APE1 indicates stabilization of a specific complex of OGG1 with 8oxoG-DNA because of a decrease in the rate of its dissociation in the presence of APE1-WT. Moreover, the observed rate constant of product release k_2 increased with the increasing concentration of APE1-WT. The increase in k_2 may indicate two possibilities: (*i*) acceleration of the catalytic step of 8oxoG base removal by OGG1 or (*ii*) stimulation of the product release step. These possibilities are in agreement with the previous observations that revealed stimulation of the

OGG1 DNA glycosylase activity by APE1 [43] as well as the evidence of active displacement of OGG1 from an abasic product by APE1 [33, 38].

To identify the contributions of the catalytic stage and the stage of dissociation to the overall process, additional experiments with DNA containing a single THF residue (referred to as an F-site) were conducted (Fig. 2*B*). The F-site cannot be cleaved by OGG1; therefore, interaction of OGG1 with FRET-F•C leads to the formation of a complex and is accompanied by an increase of the FRET signal up to 400 s. Incubation of FRET-F•C with APE1-WT alone in the presence of 1.0 mM EDTA leads to a linear increase of the FRET signal within the recorded time range indicating the cleavage of the F-site (Fig. 2*B*). Finally, the FRET-F•C substrate was preincubated with OGG1 to form the enzyme–substrate complex, and then mixed with APE1-WT. As expected, APE1-WT induces the dissociation of the OGG1–FRET-F•C complex, as reflected by a decrease of the signal up to 400 s. Of note, subsequent very slow barely noticeable growth of the FRET signal indicates the APE1-catalyzed cleavage of the F-site. Taken together, these data confirmed that APE1-WT induces dissociation of the OGG1–FRET-F•C complex. Nevertheless, these data do not contradict the possible influence of APE1-WT on the *N*-glycosidic activity of OGG1.

To gain an insight into the nature of OGG1 stimulation by APE1-WT, we carried out fluorescence measurements in the reactions of OGG1 and the FRET-8oxoG•C duplex with bacterial AP endonuclease Nfo or truncated APE1-NΔ61. First, we examined the passive mechanism of DNA glycosylase stimulation by Nfo, which is based on depletion of free AP sites generated via spontaneous dissociation of OGG1. Preincubation of OGG1 with Nfo for 15 min and subsequent mixing with the FRET-8oxoG•C substrate did not make any difference in the kinetic traces as compared to OGG1 alone (Fig. 2*A*). This result suggested that the passive stimulation of DNA glycosylase via cleavage of free AP sites cannot be detected under conditions used in the experiment. Next, we examined the effect of a

preformed nonspecific APE1-WT–DNA complex on FRET. To this end, the FRET-8oxoG•C duplex was incubated with APE1-WT and then mixed with OGG1. As shown in Fig. 2*A*, the nonspecific preformed APE1–DNA complex does not influence the amplitude of the FRET signal during DNA binding and catalysis by OGG1. This finding suggests that APE1-WT nonspecifically bound to DNA did not stimulate DNA binding by OGG1. Nevertheless, we observed an increase in the amplitude of the FRET signal in the interval 20–1000 s, indicating an increase in the catalytic activity of OGG1 or the rate of product release in the presence of APE1-WT. At the next step, the truncated APE1-NΔ61 protein was preincubated with OGG1 and then mixed with the FRET-8oxoG•C duplex. The results showed that the loss of the N-terminal domain of APE1 led to the loss of the FRET signal changes as compared to what was observed with APE1-WT (Fig. 2*A*). Taken together, these data support the hypothesis that OGG1 and APE1-WT form transient DNA-protein complexes that stabilize the interaction of OGG1 with an 8oxoG-DNA substrate and stimulate DNA-*N*-glycosylase activity of OGG1. The N-terminal domain of APE1-WT plays a key role in the formation of these complexes. Furthermore, OGG1 binds to DNA first prior to initiation of protein–protein interactions within the OGG1–APE1–DNA complex. This finding is supported by our previous kinetic analysis of AP site transfer from OGG1 to APE1-WT, where we demonstrated formation of the transient ternary complex APE1-WT–OGG1–DNA [64].

3.3. The role of the redox domain of APE1 in stimulation of uracil-DNA glycosylase activity of MBD4

MBD4 is a monofunctional DNA glycosylase that excises thymines, uracil, and 5-hydroxymethyluracil, particularly when these bases are opposite a guanine [75-76]. MBD4 belongs to the helix-hairpin-helix (HhH) DNA glycosylase superfamily, named after a conserved structural motif involved in DNA binding [77]. Just as TDG, the MBD4 protein has

a negligible turnover rate because of high affinity for the AP site generated after base excision [35]. Here, we analyzed a truncated version of MBD4: the one containing only the catalytic DNA glycosylase domain, MBD4^{cat} (residues 426–580).

To test whether APE1 can stimulate MBD4^{cat}, 50 nM 5′-^{32}P-labeled 22- and 63mer U•G duplexes were incubated with 20 nM of the catalytic domain of the MBD4^{cat} protein in BER-EDTA buffer in the presence of various concentrations of the APE1-WT and APE1-NΔ61APE1 proteins. As shown in Fig. 3*A*, incubation of U•G with MBD4^{cat} followed by piperidine treatment resulted in formation of a 9mer cleavage fragment, indicating excision of the uracil residue at position 10 (lanes 2 and 8). As expected, addition of greater amounts of the APE1-WT protein resulted in a dramatic increase in U•G cleavage and appearance of an additional faster-migrating cleavage product (lanes 3–6). These results indicated that APE1 increases AP site formation via stimulation of the turnover of MBD4^{cat}-catalyzed uracil-DNA glycosylase activity. Formation of the faster-migrating cleavage product revealed that at high protein concentrations, APE1 can cleave AP sites even in the absence of divalent cations and can generate a 9mer cleavage fragment containing a 3′-hydroxyl group (lanes 4–6). In contrast to APE1-WT, addition of increasing concentrations of the truncated mutant APE1-NΔ61 into the reaction did not cause effective stimulation of MBD4^{cat} on the U•G duplex (lanes 9–12). Similar stimulation of MBD4^{cat} by APE1-WT, but not by APE1-NΔ61, was observed when we tested a long (63mer) U•G duplex suggesting that APE1-mediated displacement of DNA glycosylase is not dependent on the length of the DNA substrate (Fig. 3B and *SI Appendix*, Fig. S4). Furthermore, in agreement with our previous observation, MBD4^{cat} excised uracil in the 63mer U•G duplex less effectively as compared to the 22mer duplex [78]. Taken together, these results showed that APE1 can stimulate turnover of MBD4^{cat} and that the redox domain of APE1 is essential for the active displacement of DNA glycosylase from an AP site in DNA.

To corroborate the function of the N-terminal domain of APE1 in MBD4^{cat} activation, we examined the processes of complex formation between MBD4^{cat} and the FRET-U•G duplex and subsequent N-glycosidic bond hydrolysis (DNA glycosylase activity) by a pre-steady-state stopped-flow assay of the FRET signal. As shown in Fig. 4, interaction of MBD4^{cat} and the FRET-U•G duplex decreased the FRET signal in the initial part of the kinetic trace (up to 100 s), indicating formation of the catalytic complex. The subsequent *N*-glycosylase reaction formed an AP site in the DNA duplex with an accompanying increase in the FRET signal in the interval 100–3000 s. Preincubation of MBD4^{cat} with APE1-WT or APE1-NΔ61 followed by mixing with the FRET-U•G substrate dramatically increased the amplitude of the FRET signal but only in the presence of APE1-WT. Just as the FRET data obtained with OGG1, these results revealed the effect of stabilization of the MBD4^{cat}–DNA complex in the presence of APE1-WT, thus pointing to the key role of the N-terminal domain of APE1 in the DNA glycosylase stimulation.

3.4. The function of the redox domain of APE1 in the stimulation of hypoxanthine-DNA glycosylase activity of ANPG

ANPG, also referred to as AAG or MPG, is a monofunctional DNA glycosylase that excises 3-methyladenine and 7-methylguanine from methylated DNA [79], hypoxanthine (Hx) [80], and 1,N^6-ethenoadenine (εA) [81-82] when present in duplex DNA. It has been reported that ANPG binds tightly to a DNA product containing an AP site after excision of Hx, and its turnover rate is accelerated by APE1 [46]. Here, we examined the role of the redox domain of APE1 in the stimulation of Hx-DNA glycosylase activity of the truncated ANPG^{cat} protein, which lacks N-terminal residues 1–73 of the full-length protein. For this purpose, 50 nM 5′-^{32}P-labeled 40mer Hx•T duplex was incubated with 15 nM ANPG^{cat} in BER-EDTA buffer in the presence of various concentrations of the APE1-WT or APE1-NΔ61

protein. As depicted in Fig. 5, incubation of Hx•T with ANPG^{cat} followed by piperidine treatment caused formation of a 19mer cleavage fragment, indicating excision of the Hx residue at position 20 (Fig. 5*A*, lanes 2 and 8). As expected, addition of a greater amount of the APE1-WT protein dramatically increased Hx•T cleavage (lanes 3–6). In contrast to OGG1 and MBD4^{cat}, we did not observe formation of a faster-migrating 19mer cleavage product containing a 3′-hydroxyl group when we used high APE1-WT protein concentrations (lanes 4–6), suggesting that ANPG^{cat} interferes with the AP site cleavage activity of APE1. As expected, addition of greater concentrations of the truncated mutant APE1-NΔ61 into the reaction did not yield effective stimulation of ANPG^{cat} on the Hx•T duplex (lanes 9–13). These results showed that the redox domain of APE1 is also essential for the stimulation of ANPG^{cat}-catalyzed Hx-DNA glycosylase activity because of active displacement of the enzyme from the AP site in DNA.

3.5. Electron microscopic analysis of DNA complexes with the APE1 protein

Biochemical evidence obtained above showed that the first 60 N-terminal residues of the redox domain together with the AP endonuclease domain of APE1 participate both in stabilization of the DNA glycosylase–substrate complex and in active disruption of the enzyme–product complex between DNA glycosylase and an AP site. To get insights into the possible mechanisms of the APE1-mediated reaction, we examined interactions between APE1 and DNA by TEM and AFM. To characterize the behavior of the APE1 protein toward DNA, we incubated full-length APE1-WT or truncated APE1-NΔ61 with an undamaged 1440-bp dsDNA fragment and then visualized DNA–protein complexes by TEM in dark-field mode using a specific spreading method (positive staining). As presented in Figure 6, APE1 bound to the normal unmodified duplex DNA in a nonspecific manner and produced protein clusters that resembled oligomer-like structures (panels b–d). Two observations point to a

cooperative mode of protein–DNA binding: (*i*) DNA molecules covered by APE1 can be observed among APE1-free DNA molecules (Fig. S5); and (ii) binding of multiple APE1 molecules to DNA and formation of protein oligomers. It is noteworthy that the nucleation of APE1 polymerization on DNA appeared to be slightly promoted by the presence of 5′ and 3′ DNA extremities (panels b1–b3). The APE1 oligomerization on DNA induced conformational distortions of DNA helix structure as shown in panels c and d. These helix distortions were sometimes drastic and could promote more densely folded molecular configurations of duplex DNA fragments (panels c [arrow] and d1). It should be noted that the presence of APE1 oligomers on DNA increased intramolecular DNA folding as observed in panels c and d and even induced intermolecular bridging among several DNA molecules thus forming small and large condensates (panels d1 and d2) possibly via protein–protein interactions across distant APE1-oligomers. When examining protein–DNA complexes with the truncated APE1-NΔ61 protein, we also observed protein oligomerization along DNA and conformational distortions of the helix (panels e1 and e2) but to a much lesser extent as compared to full-length APE1-WT. Moreover, no events of intermolecular DNA bridging in the presence of APE1-NΔ61 were observed. Taken together, these results suggested that APE1 can cooperatively bind along a normal undamaged DNA duplex and generate protein–DNA oligomeric complexes. Oligomerization of APE1 on DNA induces dramatic distortions in helix structure, and they can mediate intra- and intermolecular DNA bridging. By contrast, truncated APE1-NΔ61 oligomerized along DNA with lesser efficacy and did not induce intermolecular DNA bridging as compared to full-length APE1-WT.

To characterize DNA distortions caused by APE1, we measured the ratio of DNA contour length (s) to end-to-end distances (d) of the 1440-bp DNA fragment. The s/d ratio provides information about persistence of the DNA fragment length and conformational changes induced by APE1, for example a value >1 of the s/d ratio reflects greater DNA

curvature. The results in the histogram clearly indicate that APE1 induces conformational changes according to the increase in the s/d ratio (curvature of the DNA fragment) for the APE1–DNA complexes in comparison with the bared DNA (*SI Appendix*, Fig. S6). The s/d ratio obtained with APE1-NΔ61 is closer to that obtained with the naked DNA, confirming that APE1-NΔ61 introduces only minimal conformational changes.

3.6. Analyses of the APE1–abasic site DNA complexes on short fragments

To examine the APE1 oligomeric complexes on DNA, we incubated native APE1 with a 210-bp DNA fragment containing a single AP site in the middle of the sequence, and after immobilization on the support, the samples were subjected to AFM or TEM imaging. AFM generates topographic images of high-molecular-weight complexes, which help both to measure local deformations of DNA induced by APE1 and to visualize the oligomerization of the protein onto DNA. As shown in Figure 7, APE1 interacted with the AP site located in the middle of the DNA fragment and induced a spectacular DNA kink (panels c–f). The images also revealed that APE1 not only bound to the AP site but also polymerized along undamaged DNA segments; these in turn promoted dramatic local curvature, torsion of DNA (panels c–f). We measured the angle of curvature induced by APE1 at the abasic site on this fragment in AFM and in TEM images by a method described previously [83-84]. The distribution of the angles for sets of 100 measurements obtained by TEM is presented in Fig. 7g. We found that the presence of the abasic site induces curvature of ~30° and the presence of APE1 on this abasic site induces curvature centered around 90°. The fragments observed in the presence of APE1 are either in complex with DNA or free as indicated by the bimodal distribution. These results again revealed nonspecific association of APE1 with regular DNA, implying cooperative polymerization of APE1 along the DNA duplex. On the basis of the data obtained by visualization of the APE1 oligomer–DNA complexes by TEM and AFM, we

can say that protein oligomerization on DNA duplexes enables APE1 to move along the DNA in search of AP sites and possibly other lesions. On the other hand, the polymerization of APE1 along undamaged DNA should result in unproductive DNA substrate binding and subsequently in a decrease of the effective enzyme concentration in the reaction. This effect in turn may slow down APE1-catalyzed cleavage activities on long DNA substrates.

3.7. Effects of DNA substrate length on the APE1-catalyzed cleavage of AP site- and αdA-containing duplex oligonucleotides

Binding of APE1 to undamaged DNA and formation of stable APE1–DNA complexes may interfere with APE1-catalyzed DNA repair activities. Indeed, binding of APE1 to a DNA duplex in an unproductive way should decrease the effective enzyme concentration in the reaction. To examine this possibility, we measured cleavage efficacy of APE1 on αdA•T and THF•T duplex oligonucleotides of various lengths ranging from 17 to 64 bp. As shown in Fig. 8*A*, APE1 cleaved more than 50% of the 17mer αdA•T duplex in 10 min (lane 4), whereas the cleavage of the 64mer αdA•T duplex was barely visible even after 60-min incubation (lane 14). The cleavage efficacy of αdA•T duplexes by APE1 can be ranked in the order 17mer > 22mer > 43mer ≈ 64mer, with the extent of incision of the 17mer duplex being 3- to 18-fold greater than that of the longer DNA duplexes (Fig. 8*B*). Similar results were observed with 17mer to 64mer THF•T duplex oligonucleotides. The efficacy of APE1 cleavage of a synthetic AP site can be ranked in the order 17mer > 22mer > 43mer > 64mer, with the extent of incision of the 17mer duplex being 1.5- to 6-fold greater than that of the longer DNA duplexes (*SI Appendix*, Fig. S7). These data suggested that inhibition of the APE1-catalyzed cleavage activities on long DNA substrates may be due to stable association of the enzyme with undamaged regular DNA.

Next, we evaluated the cleavage efficacy of truncated mutant APE1-NΔ61 and *E. coli* AP endonuclease Nfo on 17- to 64mer DNA substrates. As presented in Fig. 9*A*, APE1-NΔ61 more effectively cleaved 17mer and 22mer THF•T duplexes than 43mer and 64mer ones. Nevertheless, the graph shows that the differences in the cleavage efficacy between short and long DNA oligonucleotides were less pronounced, and the error bars for all four DNA substrates overlapped substantially, pointing to a small confidence interval as compared to the results obtained with APE1-WT. Furthermore, *E. coli* AP endonuclease Nfo cleaved 22-, 43-, and 64mer αdA•T duplexes with similar efficacy and manifested only a weak preference for the 17mer substrate, contrary to APE1-WT (Fig. 9*B*). No significant differences were observed in the cleavage efficacy of Nfo acting on THF•T duplexes of various lengths (*SI Appendix*, Fig. S8). To further substantiate differences between AP endonucleases, we calculated the linear velocities of DNA cleavage (Table S1). As expected, the results showed that APE1 has a strong preference for shorter DNA fragments, whereas *E. coli* Nfo cleaves short and long DNA fragment with similar efficacy (*SI Appendix*, Fig. S9). Taken together, these results suggested that as opposed to APE1, the AP endonucleases lacking the N-terminal part of redox domain do not have a strong cleavage preference for short DNA substrates.

4. Discussion

The redox domain that spans the region between amino acid positions 35 and 127 of the major human AP endonuclease, APE1, regulates the sequence-specific DNA binding of various transcription factors [52, 85]. The existent crystal structures of APE1 in complex with DNA containing an AP site do not show any additional interactions of the N-terminal amino acid residues with a DNA duplex [86]. Indeed, the truncated APE1-NΔ61 protein has a proficient AP site cleavage activity similar to that of the full-length APE1 protein, indicating that N-terminal residues are not required for BER functions [53]. Nevertheless, the first 42 N-terminal disordered amino acid residues of APE1, not visible in crystal structures, are highly enriched in positively charged basic lysine and arginine residues, which can be engaged in electrostatic interactions with DNA phosphates. Several lines of evidence show that N-terminal amino acid residues of APE1 participate in DNA binding during NIR activity [21] and in interaction of the protein with RNA and negative calcium responsive sequence elements (nCaRE) of certain gene promoters [87-89]. The deletion, mutation, and/or acetylation of lysine residues among the first 33 amino acid residues of APE1 lead to increased AP site cleavage activity [88, 90]. Taken together, these observations point to the existence of two N- and C-terminal DNA-binding sites in the APE1 protein and that the additional interactions of the N-terminal amino acid residues of APE1 with DNA may contribute to both transcription regulation and DNA repair.

The function of the first 61 N-terminal residues of the redox domain of APE1 in the DNA glycosylase-independent NIR pathway and specific binding to DNA and RNA suggest that the redox domain was acquired during vertebrate evolution to perform additional biological functions absent in bacterial homologs such as *E. coli* exonuclease III. In the present work, we are interested in the participation of the redox domain of APE1 in the stimulation of DNA glycosylases. It has been shown that APE1 stimulates multiple turnover

of human DNA glycosylases by actively displacing them from the AP site, the end product of the reaction [36-38]. Moreover, the APE1-catalyzed stimulation does not require the AP site cleavage activity suggesting that APE1 can displace DNA glycosylases without cutting AP site in DNA [43, 46]. In addition, several studies suggest that APE1 does not interact with DNA glycosylases via specific protein–protein interactions [36, 91]. For example, the ability of APE1-WT to stimulate truncated DNA glycosylase ANPG^{cat} [present study and [46]] and even the catalytic domain of MBD4 and TDG [present study and [47]] indicates the absence of specific protein–protein contacts. This observation implies that the effect of APE1-WT is mediated by the conformational changes of DNA induced by APE1-WT. Our results here showed that the truncated APE1-NΔ61 protein deficient in redox and NIR functions cannot stimulate the repair activities of human DNA glycosylases OGG1, MBD4^{cat}, and ANPG^{cat}. All these findings reveal that the APE1-catalyzed redox function, NIR activity, and DNA glycosylase stimulation share a common underlying molecular mechanism. Here, we hypothesized that interactions of the N-terminal part of the redox domain of APE1 with DNA and conformational changes of DNA induced by APE1 binding may be involved in the disruption of the complex of a DNA glycosylase with an AP site.

To elucidate the molecular mechanism of the APE1-catalyzed stimulation, we employed the stopped-flow fluorescence analyses of the interaction of APE1 with OGG1–FRET-8oxoG•C and MBD4^{cat}–FRET-U•G complexes under the experimental conditions used (Figs. 2 and 4). It is known that the DNA damage recognition by a DNA glycosylase involves several key steps: (*i*) nonspecific DNA binding; (*ii*) DNA bending at the lesion site, (*iii*) eversion of the damaged base from the double helix into the enzyme's active site, and (*iv*) insertion of some amino acids of the enzyme into the resulting void in DNA. It is clear that certain steps may influence stability of the DNA duplex, which in turn would affect the distance between the fluorophores on DNA and produce a change in the FRET signal. Most

likely, stabilization of the ends of the DNA duplex, which affects the distance between the fluorophores, occurs already at the first step of a nonspecific enzyme–substrate complex formation. Based on this assumption, the FRET data revealed no difference in the observed rate constant (k_1) of the formation of nonspecific DNA glycosylase–DNA substrate complex in the presence or absence of APE1. The dramatic change in FRET signal amplitude in the presence of APE-WT after initial DNA glycosylase substrate binding suggests that APE1 influences subsequent steps of catalytic enzyme–substrate complex formation such as DNA bending, damaged base flipping out, and insertion of amino acid residues (Figs. 2 and 4). The action of APE1 stabilizes these intermediate transition states of the DNA damage-specific binding by DNA glycosylases. This APE1-mediated stabilization of the DNA glycosylase-specific interactions with DNA damage results in more effective accumulation of the catalytically proficient enzyme–substrate complexes. The same DNA distortions caused by APE1 may lead to expulsion of the DNA glycosylases from abasic site DNA owing to the loss of "anchor" interactions between an everted damaged base and the enzyme active site, which in turn may increase turnover rates of the enzymes. Overall, these data support the hypothesis that APE1 forms a transient complex with DNA and that this APE1–DNA complex does not accelerate nonspecific DNA binding by DNA glycosylases but stabilizes intermediate stages of catalysis between a DNA glycosylase and its DNA substrate. The nature of the stabilization effect is probably related to DNA helix distortion by APE1, which facilitates bypassing of certain steps of catalytic complex formation by a DNA glycosylase, for example, DNA bending and flipping out of the damaged base. Due to acceleration of catalytic complex formation steps, we observed an increase in the rate of catalytic reaction of DNA glycosylases. The loss of the N-terminal domain of APE1-WT leads to a loss of both stabilization of the enzyme–substrate complex and active disruption of the enzyme–product complex and thereby of the ability to modulate DNA-*N*-glycosylase activity.

Here, we performed TEM and AFM imaging to study APE1–DNA interactions. The results showed that APE1 can dynamically polymerize on DNA in an apparently sequence-independent manner. We propose that this protein polymerization allows for scanning of the structural properties of DNA with short residence time, in order to search for abasic sites. Cooperative oligomerization of proteins along a DNA duplex is well known for recombinases (RecA and Rad51) and for other proteins such as HNS, Stpa, LrpC, and Fur [65, 92-93]. Such protein polymerization onto DNA is related to various functions and is referred to as "collaborative protein filaments" [92]. A DNA duplex containing an AP site manifests local flexibility, which is recognized by APE1. We demonstrated that APE1 can stabilize a kink, specific structure of the DNA duplex, as it was previously shown for PARP1 on a single-strand break [83] and for MC1 on its DNA-binding site [84, 94]. We propose that the APE1 oligomer functions as a sensor of conformational properties of DNA and this new function of APE1 allows for scanning of DNA and enables the search for local DNA structural perturbations such as an AP site and other DNA lesions.

The finding that multiple APE1 proteins can be stably associated with an undamaged DNA duplex implies a decrease in the effective enzyme concentrations in solution, which in turn should lower enzymatic activities on long DNA substrates. In line with this notion, we observed a dramatic decrease in APE1-catalyzed cleavage activities on 64mer DNA substrates as compared to 17mer ones. Furthermore, the efficacy of AP site and αdA-DNA cleavage by APE1 can be ranked in the order 17mer > 22mer > 43mer > 64mer, strictly depending on the size of DNA fragments. Contrary to full-length APE1, the truncated APE1-NΔ61 protein manifested only a slight preference for short DNA duplexes as compared to long ones. Besides, *E. coli* AP endonuclease Nfo did not discriminate between DNA substrates of various length and cleaved 17–64mer duplexes with more or less similar efficacy. These data are in agreement with TEM and AFM imaging, which revealed that full-length APE1 tends to

polymerize on DNA fragments, thus generating protein oligomers along DNA fragments. Altogether, these results suggest that the first 61 N-terminal residues of APE1 participate in protein polymerization along DNA and in formation of oligomerlike complexes by binding to undamaged DNA via electrostatic interactions between DNA phosphates and positively charged basic lysine and arginine residues.

Under our experimental conditions, APE1 preferentially binds to the DNA duplex termini possibly because of the presence of transient single-stranded (ss) DNA generated by helix breathing at its extremities. Nevertheless, the population of APE1 oligomers at DNA duplex termini is much smaller as compared to APE1 oligomers bound along DNA fragment. We can theorize that in the context of unbroken DNA chromosomes, APE1 mainly binds to nucleosome-free DNA either in the sequence-specific manner for example to an nCaRE regulatory element, or to ssDNA generated during DNA transcription and replication. Here we propose that the APE1-oligomers on DNA perform both functions: stabilize the catalytic complex between the DNA glycosylases and their DNA substrates and disrupt the enzyme–end product complex. Furthermore, the APE1-catalyzed oligomerization on DNA may also serve as a molecular mechanism behind the redox function of APE1. It is tempting to speculate that APE1 oligomers on DNA induce distortions in helix structure, and these conformational changes may influence the affinity of transcription factors for cognate DNA sequences.

On the basis of our data, we can formulate a model in which APE1 binds to the DNA duplex termini in a stable manner and then recruits other APE1 molecules to bind nearby in a cooperative manner, which in turn initiates polymerization of the APE1 proteins along DNA, thus generating APE1-oligomers seen in TEM and AFM images (Fig. 10). Upon initial binding of DNA glycosylases to their substrates in the absence of APE1, the mutual “induced-fit” steps shift the conformational ensemble toward the transition state. APE1 oligomers

mediate conformational changes in the DNA duplex, which may mimic the conformation of the transition state of the reaction, thereby lowering the entropic barrier and stabilizing the enzyme–substrate complex. In the equilibrium association of a DNA glycosylase with a damaged site in DNA, the rate constant of the forward reaction is close to a diffusion-controlled value, but when the DNA substrate is bound to APE1, it is preformed for the formation of a catalytically competent complex with DNA glycosylase. Consequently, the rate constant of the reverse reaction should be lower in comparison with the APE1-free case. By contrast, in the complex of DNA glycosylase with the end product (AP site), the dissociation rate constant is higher for the AP site associated with APE1 owing to distortion of DNA structure, which decreases the number of specific contacts between DNA glycosylase and AP site DNA. Overall, we can say that APE1-catalyzed stimulation of certain DNA glycosylases is based on the transformation of an “induced-fit” into a “conformational selection” mechanism. Finally, APE1-induced conformational changes in DNA helix stimulate (i) formation of a catalytically competent enzyme–substrate complex, (ii) disruption of the DNA glycosylase–end product complex, and (iii) probably the binding of redox-dependent transcription factors to DNA. We propose that the redox domain of an AP endonuclease, acquired during evolution of vertebrates, provides additional biological functions including redox and DNA glycosylase stimulation. In the process of natural evolution, these additional functions of APE1 have become essential for cellular proliferation and embryonic development in mammals.

Acknowledgements

This work was supported by grants from la Ligue Nationale Française Contre le Cancer « Equipe LNCC 2016 » and Electricité de France RB 2016-17 (to M.S.), Science Committee of the Ministry of Education and Science of the Republic of Kazakhstan, Program 0212/PTF-14-OT and grant 3755/GF4 (to B.T.M.), the Federal Agency of Scientific Organizations VI.57.1.2/0309-2016-0001 (to N.A.K.). ELC was supported by grants from CNano Ile de France, Plan Cancer Inserm, and Paris Sud University (MRM). The pre-steady-state kinetic studies of MBD4 were supported by the Russian Science Foundation (grant #16-14-10038 to O.S.F.). O.K. and M.B. were supported by the fellowships from the Russian Foundation for Basic Research #16-04-00037) and Poland, respectively. The funders had no role in study design, data collection and analysis, decision to publish, or preparation of the manuscript.

References

[1] D.E. Barnes, T. Lindahl, Repair and genetic consequences of endogenous DNA base damage in mammalian cells, Annu. Rev. Genet., 38 (2004) 445-476.
[2] H.E. Krokan, M. Bjoras, Base excision repair, Cold Spring Harb. Perspect. Biol., 5 (2013) a012583.
[3] A. Yasui, Alternative excision repair pathways, Cold Spring Harb. Perspect. Biol., 5 (2013) 1-8.
[4] A.A. Ischenko, M.K. Saparbaev, Alternative nucleotide incision repair pathway for oxidative DNA damage, Nature, 415 (2002) 183-187.
[5] A.L. Jacobs, P. Schar, DNA glycosylases: in DNA repair and beyond, Chromosoma, (2011).
[6] C.Y. Lee, J.C. Delaney, M. Kartalou, G.M. Lingaraju, A. Maor-Shoshani, J.M. Essigmann, L.D. Samson, Recognition and processing of a new repertoire of DNA substrates by human 3-methyladenine DNA glycosylase (AAG), Biochemistry, 48 (2009) 1850-1861.
[7] A. Bellacosa, A.C. Drohat, Role of base excision repair in maintaining the genetic and epigenetic integrity of CpG sites, DNA Repair (Amst), 32 (2015) 33-42.
[8] D.O. Zharkov, T.A. Rosenquist, S.E. Gerchman, A.P. Grollman, Substrate specificity and reaction mechanism of murine 8-oxoguanine-DNA glycosylase, J Biol Chem, 275 (2000) 28607-28617.
[9] A. Prakash, S. Doublie, S.S. Wallace, The Fpg/Nei family of DNA glycosylases: substrates, structures, and search for damage, Prog Mol Biol Transl Sci, 110 (2012) 71-91.
[10] T.K. Hazra, Y.W. Kow, Z. Hatahet, B. Imhoff, I. Boldogh, S.K. Mokkapati, S. Mitra, T. Izumi, Identification and characterization of a novel human DNA glycosylase for repair of cytosine-derived lesions, J. Biol. Chem., 277 (2002) 30417-30420.
[11] V. Bandaru, S. Sunkara, S.S. Wallace, J.P. Bond, A novel human DNA glycosylase that removes oxidative DNA damage and is homologous to *Escherichia coli* endonuclease VIII, DNA Repair (Amst), 1 (2002) 517-529.
[12] S.Z. Krokeide, J.K. Laerdahl, M. Salah, L. Luna, F.H. Cederkvist, A.M. Fleming, C.J. Burrows, B. Dalhus, M. Bjoras, Human NEIL3 is mainly a monofunctional DNA glycosylase removing spiroimindiohydantoin and guanidinohydantoin, DNA Repair (Amst), 12 (2013) 1159-1164.
[13] R.P. Cunningham, DNA glycosylases, Mutat. Res., 383 (1997) 189-196.
[14] M.L. Dodson, M.L. Michaels, R.S. Lloyd, Unified catalytic mechanism for DNA glycosylases, J. Biol. Chem., 269 (1994) 32709-32712.
[15] B. Demple, L. Harrison, Repair of oxidative damage to DNA: enzymology and biology, Annu. Rev. Biochem., 63 (1994) 915-948.
[16] A. Das, L. Wiederhold, J.B. Leppard, P. Kedar, R. Prasad, H. Wang, I. Boldogh, F. Karimi-Busheri, M. Weinfeld, A.E. Tomkinson, S.H. Wilson, S. Mitra, T.K. Hazra, NEIL2-initiated, APE-independent repair of oxidized bases in DNA: Evidence for a repair complex in human cells, DNA Repair (Amst), 5 (2006) 1439-1448.
[17] J.C. Fromme, A. Banerjee, G.L. Verdine, DNA glycosylase recognition and catalysis, Curr. Opin. Struct. Biol., 14 (2004) 43-49.
[18] D.O. Zharkov, Base excision DNA repair, Cell. Mol. Life Sci., 65 (2008) 1544-1565.
[19] H. Ide, K. Tedzuka, H. Shimzu, Y. Kimura, A.A. Purmal, S.S. Wallace, Y.W. Kow, Alpha-deoxyadenosine, a major anoxic radiolysis product of adenine in DNA, is a substrate for *Escherichia coli* endonuclease IV, Biochemistry, 33 (1994) 7842-7847.
[20] A.A. Ishchenko, H. Ide, D. Ramotar, G. Nevinsky, M. Saparbaev, Alpha-anomeric deoxynucleotides, anoxic products of ionizing radiation, are substrates for the endonuclease IV-type AP endonucleases, Biochemistry, 43 (2004) 15210-15216.
[21] L. Gros, A.A. Ishchenko, H. Ide, R.H. Elder, M.K. Saparbaev, The major human AP endonuclease (Ape1) is involved in the nucleotide incision repair pathway, Nucleic Acids Res., 32 (2004) 73-81.
[22] M. Redrejo-Rodriguez, C. Saint-Pierre, S. Couve, A. Mazouzi, A.A. Ishchenko, D. Gasparutto, M. Saparbaev, New insights in the removal of the hydantoins, oxidation product of pyrimidines, via the base excision and nucleotide incision repair pathways, PLoS One, 6 (2011) e21039.
[23] B. Demple, J.S. Sung, Molecular and biological roles of Ape1 protein in mammalian base excision repair, DNA Repair (Amst), 4 (2005) 1442-1449.
[24] G. Tell, D.M. Wilson, 3rd, C.H. Lee, Intrusion of a DNA repair protein in the RNome world: is this the beginning of a new era?, Mol. Cell. Biol., 30 (2010) 366-371.

[25] E. Yu, S.P. Gaucher, M.Z. Hadi, Probing conformational changes in Ape1 during the progression of base excision repair, Biochemistry, 49 (2010) 3786-3796.
[26] S. Daviet, S. Couve-Privat, L. Gros, K. Shinozuka, H. Ide, M. Saparbaev, A.A. Ishchenko, Major oxidative products of cytosine are substrates for the nucleotide incision repair pathway, DNA Repair (Amst), 6 (2007) 8-18.
[27] P.P. Christov, S. Banerjee, M.P. Stone, C.J. Rizzo, Selective Incision of the alpha-N-Methyl-Formamidopyrimidine Anomer by Escherichia coli Endonuclease IV, J. Nucleic. Acids., 2010 (2010).
[28] P. Prorok, D. Alili, C. Saint-Pierre, D. Gasparutto, D.O. Zharkov, A.A. Ishchenko, B. Tudek, M.K. Saparbaev, Uracil in duplex DNA is a substrate for the nucleotide incision repair pathway in human cells, Proc Natl Acad Sci U S A, 110 (2013) E3695-3703.
[29] P. Prorok, C. Saint-Pierre, D. Gasparutto, O.S. Fedorova, A.A. Ishchenko, H. Leh, M. Buckle, B. Tudek, M. Saparbaev, Highly mutagenic exocyclic DNA adducts are substrates for the human nucleotide incision repair pathway, PLoS One, 7 (2012) e51776.
[30] A.B. Guliaev, B. Hang, B. Singer, Structural insights by molecular dynamics simulations into specificity of the major human AP endonuclease toward the benzene-derived DNA adduct, pBQ-C, Nucleic Acids Res., 32 (2004) 2844-2852.
[31] M.G. Vrouwe, A. Pines, R.M. Overmeer, K. Hanada, L.H. Mullenders, UV-induced photolesions elicit ATR-kinase-dependent signaling in non-cycling cells through nucleotide excision repair-dependent and -independent pathways, J. Cell Sci., 124 (2011) 435-446.
[32] O.D. Scharer, H.M. Nash, J. Jiricny, J. Laval, G.L. Verdine, Specific binding of a designed pyrrolidine abasic site analog to multiple DNA glycosylases, J. Biol. Chem., 273 (1998) 8592-8597.
[33] J.W. Hill, T.K. Hazra, T. Izumi, S. Mitra, Stimulation of human 8-oxoguanine-DNA glycosylase by AP-endonuclease: potential coordination of the initial steps in base excision repair, Nucleic Acids Res., 29 (2001) 430-438.
[34] T.R. Waters, P.F. Swann, Kinetics of the action of thymine DNA glycosylase, J. Biol. Chem., 273 (1998) 20007-20014.
[35] F. Petronzelli, A. Riccio, G.D. Markham, S.H. Seeholzer, J. Stoerker, M. Genuardi, A.T. Yeung, Y. Matsumoto, A. Bellacosa, Biphasic kinetics of the human DNA repair protein MED1 (MBD4), a mismatch-specific DNA N-glycosylase, J. Biol. Chem., 275 (2000) 32422-32429.
[36] T.R. Waters, P. Gallinari, J. Jiricny, P.F. Swann, Human thymine DNA glycosylase binds to apurinic sites in DNA but is displaced by human apurinic endonuclease 1, J. Biol. Chem., 274 (1999) 67-74.
[37] L. Xia, L. Zheng, H.W. Lee, S.E. Bates, L. Federico, B. Shen, T.R. O'Connor, Human 3-methyladenine-DNA glycosylase: effect of sequence context on excision, association with PCNA, and stimulation by AP endonuclease, J Mol Biol, 346 (2005) 1259-1274.
[38] V.S. Sidorenko, G.A. Nevinsky, D.O. Zharkov, Mechanism of interaction between human 8-oxoguanine-DNA glycosylase and AP endonuclease, DNA Repair (Amst), 6 (2007) 317-328.
[39] A. Esadze, G. Rodriguez, S.L. Cravens, J.T. Stivers, AP-Endonuclease 1 Accelerates Turnover of Human 8-Oxoguanine DNA Glycosylase by Preventing Retrograde Binding to the Abasic-Site Product, Biochemistry, 56 (2017) 1974-1986.
[40] D.S. Chen, T. Herman, B. Demple, Two distinct human DNA diesterases that hydrolyze 3'-blocking deoxyribose fragments from oxidized DNA, Nucleic Acids Res., 19 (1991) 5907-5914.
[41] J.K. Horton, D.K. Srivastava, B.Z. Zmudzka, S.H. Wilson, Strategic down-regulation of DNA polymerase beta by antisense RNA sensitizes mammalian cells to specific DNA damaging agents, Nucleic Acids Res, 23 (1995) 3810-3815.
[42] B. Doseth, T. Visnes, A. Wallenius, I. Ericsson, A. Sarno, H.S. Pettersen, A. Flatberg, T. Catterall, G. Slupphaug, H.E. Krokan, B. Kavli, Uracil-DNA glycosylase in base excision repair and adaptive immunity: species differences between man and mouse, J Biol Chem, 286 (2011) 16669-16680.
[43] A.E. Vidal, I.D. Hickson, S. Boiteux, J.P. Radicella, Mechanism of stimulation of the DNA glycosylase activity of hOGG1 by the major human AP endonuclease: bypass of the AP lyase activity step, Nucleic Acids Res., 29 (2001) 1285-1292.
[44] U. Hardeland, M. Bentele, T. Lettieri, R. Steinacher, J. Jiricny, P. Schar, Thymine DNA glycosylase, Prog Nucleic Acid Res Mol Biol, 68 (2001) 235-253.

[45] S.S. Parikh, C.D. Mol, G. Slupphaug, S. Bharati, H.E. Krokan, J.A. Tainer, Base excision repair initiation revealed by crystal structures and binding kinetics of human uracil-DNA glycosylase with DNA, Embo J, 17 (1998) 5214-5226.
[46] M.R. Baldwin, P.J. O'Brien, Human AP endonuclease 1 stimulates multiple-turnover base excision by alkyladenine DNA glycosylase, Biochemistry, 48 (2009) 6022-6033.
[47] M.E. Fitzgerald, A.C. Drohat, Coordinating the initial steps of base excision repair. Apurinic/apyrimidinic endonuclease 1 actively stimulates thymine DNA glycosylase by disrupting the product complex, J. Biol. Chem., 283 (2008) 32680-32690.
[48] B. Demple, T. Herman, D.S. Chen, Cloning and expression of APE, the cDNA encoding the major human apurinic endonuclease: definition of a family of DNA repair enzymes, Proc. Natl. Acad. Sci. U. S. A., 88 (1991) 11450-11454.
[49] C.N. Robson, A.M. Milne, D.J. Pappin, I.D. Hickson, Isolation of cDNA clones encoding an enzyme from bovine cells that repairs oxidative DNA damage in vitro: homology with bacterial repair enzymes, Nucleic Acids Res., 19 (1991) 1087-1092.
[50] S. Xanthoudakis, G. Miao, F. Wang, Y.C. Pan, T. Curran, Redox activation of Fos-Jun DNA binding activity is mediated by a DNA repair enzyme, Embo J., 11 (1992) 3323-3335.
[51] C. Abate, L. Patel, F.J. Rauscher, 3rd, T. Curran, Redox regulation of fos and jun DNA-binding activity in vitro, Science, 249 (1990) 1157-1161.
[52] S. Xanthoudakis, G.G. Miao, T. Curran, The redox and DNA-repair activities of Ref-1 are encoded by nonoverlapping domains, Proc. Natl. Acad. Sci. U. S. A., 91 (1994) 23-27.
[53] T. Izumi, S. Mitra, Deletion analysis of human AP-endonuclease: minimum sequence required for the endonuclease activity, Carcinogenesis, 19 (1998) 525-527.
[54] S. Xanthoudakis, R.J. Smeyne, J.D. Wallace, T. Curran, The redox/DNA repair protein, Ref-1, is essential for early embryonic development in mice, Proc. Natl. Acad. Sci. U. S. A., 93 (1996) 8919-8923.
[55] H. Fung, B. Demple, A vital role for Ape1/Ref1 protein in repairing spontaneous DNA damage in human cells, Mol. Cell, 17 (2005) 463-470.
[56] T. Izumi, D.B. Brown, C.V. Naidu, K.K. Bhakat, M.A. Macinnes, H. Saito, D.J. Chen, S. Mitra, Two essential but distinct functions of the mammalian abasic endonuclease, Proc. Natl. Acad. Sci. U. S. A., 102 (2005) 5739-5743.
[57] S. Madlener, T. Strobel, S. Vose, O. Saydam, B.D. Price, B. Demple, N. Saydam, Essential role for mammalian apurinic/apyrimidinic (AP) endonuclease Ape1/Ref-1 in telomere maintenance, Proc. Natl. Acad. Sci. U. S. A., 110 (2013) 17844-17849.
[58] M. Saparbaev, S. Langouet, C.V. Privezentzev, F.P. Guengerich, H. Cai, R.H. Elder, J. Laval, 1,N(2)-ethenoguanine, a mutagenic DNA adduct, is a primary substrate of Escherichia coli mismatch-specific uracil-DNA glycosylase and human alkylpurine-DNA-N-glycosylase, J. Biol. Chem., 277 (2002) 26987-26993.
[59] N.A. Kuznetsov, V.V. Koval, D.O. Zharkov, G.A. Nevinsky, K.T. Douglas, O.S. Fedorova, Kinetics of substrate recognition and cleavage by human 8-oxoguanine-DNA glycosylase, Nucleic Acids Res., 33 (2005) 3919-3931.
[60] S. Morera, I. Grin, A. Vigouroux, S. Couve, V. Henriot, M. Saparbaev, A.A. Ishchenko, Biochemical and structural characterization of the glycosylase domain of MBD4 bound to thymine and 5-hydroxymethyuracil-containing DNA, Nucleic Acids Res., 40 (2012) 9917-9926.
[61] A.A. Ishchenko, E. Deprez, A. Maksimenko, J.C. Brochon, P. Tauc, M.K. Saparbaev, Uncoupling of the base excision and nucleotide incision repair pathways reveals their respective biological roles, Proc. Natl. Acad. Sci. U. S. A., 103 (2006) 2564-2569.
[62] Z. Akishev, S. Taipakova, B. Joldybayeva, C. Zutterling, I. Smekenov, A.A. Ishchenko, D.O. Zharkov, A.K. Bissenbaev, M. Saparbaev, The major Arabidopsis thaliana apurinic/apyrimidinic endonuclease, ARP is involved in the plant nucleotide incision repair pathway, DNA Repair (Amst), 48 (2016) 30-42.
[63] N.A. Kuznetsov, O.A. Kladova, A.A. Kuznetsova, A.A. Ishchenko, M.K. Saparbaev, D.O. Zharkov, O.S. Fedorova, Conformational Dynamics of DNA Repair by Escherichia coli Endonuclease III, Journal of Biological Chemistry, 290 (2015) 14338-14349.

[64] A.A. Kuznetsova, N.A. Kuznetsov, A.A. Ishchenko, M.K. Saparbaev, O.S. Fedorova, Pre-steady-state fluorescence analysis of damaged DNA transfer from human DNA glycosylases to AP endonuclease APE1, Biochimica Et Biophysica Acta-General Subjects, 1840 (2014) 3042-3051.
[65] C. Beloin, J. Jeusset, B. Revet, G. Mirambeau, F. Le Hegarat, E. Le Cam, Contribution of DNA conformation and topology in right-handed DNA wrapping by the Bacillus subtilis LrpC protein, J. Biol. Chem., 278 (2003) 5333-5342.
[66] D. Pastre, O. Pietrement, S. Fusil, F. Landousy, J. Jeusset, M.O. David, L. Hamon, E. Le Cam, A. Zozime, Adsorption of DNA to mica mediated by divalent counterions: a theoretical and experimental study, Biophys. J., 85 (2003) 2507-2518.
[67] A.D. Miroshnikova, A.A. Kuznetsova, Y.N. Vorobjev, N.A. Kuznetsov, O.S. Fedorova, Effects of mono- and divalent metal ions on DNA binding and catalysis of human apurinic/apyrimidinic endonuclease 1, Mol Biosyst, 12 (2016) 1527-1539.
[68] N.A. Timofeyeva, V.V. Koval, D.G. Knorre, D.O. Zharkov, M.K. Saparbaev, A.A. Ishchenko, O.S. Fedorova, Conformational dynamics of human AP endonuclease in base excision and nucleotide incision repair pathways, J. Biomol. Struct. Dyn., 26 (2009) 637-652.
[69] S.D. Bruner, D.P. Norman, G.L. Verdine, Structural basis for recognition and repair of the endogenous mutagen 8-oxoguanine in DNA, Nature, 403 (2000) 859-866.
[70] A.A. Kuznetsova, N.A. Kuznetsov, A.A. Ishchenko, M.K. Saparbaev, O.S. Fedorova, Step-by-step mechanism of DNA damage recognition by human 8-oxoguanine DNA glycosylase, Biochim Biophys Acta, 1840 (2014) 387-395.
[71] N.A. Kuznetsov, A.A. Kuznetsova, Y.N. Vorobjev, L.N. Krasnoperov, O.S. Fedorova, Thermodynamics of the DNA damage repair steps of human 8-oxoguanine DNA glycosylase, PLoS One, 9 (2014) e98495.
[72] N.A. Kuznetsov, V.V. Koval, G.A. Nevinsky, K.T. Douglas, D.O. Zharkov, O.S. Fedorova, Kinetic conformational analysis of human 8-oxoguanine-DNA glycosylase, J. Biol. Chem., 282 (2007) 1029-1038.
[73] N.A. Kuznetsov, C. Bergonzo, A.J. Campbell, H. Li, G.V. Mechetin, C. de los Santos, A.P. Grollman, O.S. Fedorova, D.O. Zharkov, C. Simmerling, Active destabilization of base pairs by a DNA glycosylase wedge initiates damage recognition, Nucleic Acids Res, 43 (2015) 272-281.
[74] J.P. Radicella, C. Dherin, C. Desmaze, M.S. Fox, S. Boiteux, Cloning and characterization of hOGG1, a human homolog of the OGG1 gene of Saccharomyces cerevisiae, Proc. Natl. Acad. Sci. U. S. A., 94 (1997) 8010-8015.
[75] B. Hendrich, U. Hardeland, H.H. Ng, J. Jiricny, A. Bird, The thymine glycosylase MBD4 can bind to the product of deamination at methylated CpG sites, Nature, 401 (1999) 301-304.
[76] S. Cortellino, J. Xu, M. Sannai, R. Moore, E. Caretti, A. Cigliano, M. Le Coz, K. Devarajan, A. Wessels, D. Soprano, L.K. Abramowitz, M.S. Bartolomei, F. Rambow, M.R. Bassi, T. Bruno, M. Fanciulli, C. Renner, A.J. Klein-Szanto, Y. Matsumoto, D. Kobi, I. Davidson, C. Alberti, L. Larue, A. Bellacosa, Thymine DNA glycosylase is essential for active DNA demethylation by linked deamination-base excision repair, Cell, 146 (2011) 67-79.
[77] M.M. Thayer, H. Ahern, D. Xing, R.P. Cunningham, J.A. Tainer, Novel DNA binding motifs in the DNA repair enzyme endonuclease III crystal structure, Embo J., 14 (1995) 4108-4120.
[78] D.A. Yakovlev, A.A. Kuznetsova, O.S. Fedorova, N.A. Kuznetsov, Search for Modified DNA Sites with the Human Methyl-CpG-Binding Enzyme MBD4, Acta Naturae, 9 (2017) 88-98.
[79] T.R. O'Connor, J. Laval, Human cDNA expressing a functional DNA glycosylase excising 3-methyladenine and 7-methylguanine, Biochem Biophys Res Commun, 176 (1991) 1170-1177.
[80] M. Saparbaev, J. Laval, Excision of hypoxanthine from DNA containing dIMP residues by the Escherichia coli, yeast, rat, and human alkylpurine DNA glycosylases, Proc Natl Acad Sci U S A, 91 (1994) 5873-5877.
[81] M. Saparbaev, K. Kleibl, J. Laval, Escherichia coli, Saccharomyces cerevisiae, rat and human 3-methyladenine DNA glycosylases repair 1,N6-ethenoadenine when present in DNA, Nucleic Acids Res, 23 (1995) 3750-3755.
[82] B. Singer, A. Antoccia, A.K. Basu, M.K. Dosanjh, H. Fraenkel-Conrat, P.E. Gallagher, J.T. Kusmierek, Z.H. Qiu, B. Rydberg, Both purified human 1,N6-ethenoadenine-binding protein and purified human 3-methyladenine-DNA glycosylase act on 1,N6-ethenoadenine and 3-methyladenine, Proc Natl Acad Sci U S A, 89 (1992) 9386-9390.

[83] E. Le Cam, F. Fack, J. Menissier-de Murcia, J.A. Cognet, A. Barbin, V. Sarantoglou, B. Revet, E. Delain, G. de Murcia, Conformational analysis of a 139 base-pair DNA fragment containing a single-stranded break and its interaction with human poly(ADP-ribose) polymerase, J Mol Biol, 235 (1994) 1062-1071.
[84] E.L. Cam, F. Culard, E. Larquet, E. Delain, J.A. Cognet, DNA bending induced by the archaebacterial histone-like protein MC1, J. Mol. Biol., 285 (1999) 1011-1021.
[85] M.M. Georgiadis, M. Luo, R.K. Gaur, S. Delaplane, X. Li, M.R. Kelley, Evolution of the redox function in mammalian apurinic/apyrimidinic endonuclease, Mutat. Res., 643 (2008) 54-63.
[86] C.D. Mol, T. Izumi, S. Mitra, J.A. Tainer, DNA-bound structures and mutants reveal abasic DNA binding by APE1 and DNA repair coordination [corrected], Nature, 403 (2000) 451-456.
[87] K.K. Bhakat, T. Izumi, S.H. Yang, T.K. Hazra, S. Mitra, Role of acetylated human AP-endonuclease (APE1/Ref-1) in regulation of the parathyroid hormone gene, Embo J, 22 (2003) 6299-6309.
[88] D. Fantini, C. Vascotto, D. Marasco, C. D'Ambrosio, M. Romanello, L. Vitagliano, C. Pedone, M. Poletto, L. Cesaratto, F. Quadrifoglio, A. Scaloni, J.P. Radicella, G. Tell, Critical lysine residues within the overlooked N-terminal domain of human APE1 regulate its biological functions, Nucleic Acids Res, 38 (2010) 8239-8256.
[89] G. Antoniali, L. Lirussi, C. D'Ambrosio, F. Dal Piaz, C. Vascotto, E. Casarano, D. Marasco, A. Scaloni, F. Fogolari, G. Tell, SIRT1 gene expression upon genotoxic damage is regulated by APE1 through nCaRE-promoter elements, Mol Biol Cell, 25 (2014) 532-547.
[90] L. Lirussi, G. Antoniali, C. Vascotto, C. D'Ambrosio, M. Poletto, M. Romanello, D. Marasco, M. Leone, F. Quadrifoglio, K.K. Bhakat, A. Scaloni, G. Tell, Nucleolar accumulation of APE1 depends on charged lysine residues that undergo acetylation upon genotoxic stress and modulate its BER activity in cells, Mol Biol Cell, 23 (2012) 4079-4096.
[91] M.R. Baldwin, P.J. O'Brien, Defining the functional footprint for recognition and repair of deaminated DNA, Nucleic Acids Res, 40 (2012) 11638-11647.
[92] D. Ghosal, J. Lowe, Collaborative protein filaments, Embo J, 34 (2015) 2312-2320.
[93] E. Le Cam, D. Frechon, M. Barray, A. Fourcade, E. Delain, Observation of binding and polymerization of Fur repressor onto operator-containing DNA with electron and atomic force microscopes, Proc Natl Acad Sci U S A, 91 (1994) 11816-11820.
[94] F. Toulme, E. Le Cam, C. Teyssier, E. Delain, P. Sautiere, J.C. Maurizot, F. Culard, Conformational changes of DNA minicircles upon the binding of the archaebacterial histone-like protein MC1, J Biol Chem, 270 (1995) 6286-6291.

Table 1. Sequences of oligonucleotides bearing a single base lesion used to identify the BER and NIR activities and relative efficiency of the APE1-catalyzed cleavage of duplex DNA substrates.

Name	Sequence	Length (lesion position)
X-40[a]	d(AATTGCTATCTAGCTCCGC**X**CGCTGGTACCCATCTCATGA)	40 (20)
U-22[b]	d(CACTTCGGA**U**TGTGACTGATCC)	22 (12)
U-63	d(ACAGCACCAGATTCAGCAATTAAGCTCTAAG**U**CATCCGCAAAAATGACCTCTTATCAAAAGGA)	63 (32)
Y-64[c]	d(AGATTCAACTTAGTAGACGGC*CACTTCGGA***Y***TGTGACTGATCC*GGTACGACTACTAGCTTATGC)	64 (31)
Y-43	d(AGTAGACGGC*CACTTCGGA***Y***TGTGACTGATCC*GGTACGACTAC)	43 (20)
Y-22	d(CACTTCGGA**Y**TGTGACTGATCC)	22 (10)
Y-17	d(ACTTCGGA**Y**TGTGACTG)	17 (9)
c40N[d]	d(TCATGAGATGGGTACCAGCG**N**GCGGAGCTAGATAGCAATT) (complementary to X-40)	40
c22G	d(GGATCAGTCACA**G**TCCGAAGTG) (complementary to U-22)	22
c63G	d(TCCTTTTGATAAGAGGTCATTTTTGCGGATG**G**CTTAGAGCTTAATTGCTGAATCTGGTGCTGT) (complementary to U-63)	63
c64T	d(GCATAAGCTAGTAGTCGTACCGGATCAGTCACA**T**TCCGAAGTGGCCGTCTACTAAGTTGAATCT) (complementary to Y-64)	64
c43T	d(GTAGTCGTACCGGATCAGTCACA**T**TCCGAAGTGGCCGTCTACT) (complementary to Y-43)	43
c22T	d(GGATCAGTCACA**T**TCCGAAGTG) (complementary to Y-22)	22
c17T	d(CAGTCACA**T**TCCGAAGT) (complementary to Y-17)	17
FRET-Z•C[e]	5′-**FAM**- GCTCA**Z**GTACAGAGCTG-3′ 3′-**BHQ1**-CGAGT**C**CATGTCTCGAC-5′	17 (6)
FRET-U•G	5′-**FAM**- GCTCA **U** GTACAGAGCTG-3′	17 (6)

	3′-**BHQ1**-CGAGT **G** CATGTCTCGAC-5′	

[a]X is either 8oxoG, U or Hx;
[b]U is for Uracil;
[c]Y is either THF or αdA;
[d]N is either G, A, T or C;
[e]Z is either 8oxoG or THF;
FAM is for 6-carboxyfluorescein;
BHQ1 is for black hole quencher.

FIGURE LEGENDS

Figure 1. **Stimulation of human-OGG1–catalyzed DNA glycosylase activity by APE1 WT or mutant proteins**. (*A*) Denaturing PAGE analysis of the cleavage products. In brief, 50 nM 5′-^{32}P-labeled 40mer 8oxoG•C duplex oligonucleotide was incubated in BER-EDTA reaction buffer for 30 min at 37°C in the presence of 15 nM OGG1 and various concentrations of APE1-WT or truncated APE1-NΔ61 mutant. Lanes 1 and 8, 8oxoG•C duplex; lanes 2 and 9, as in lane 1 but 15 nM OGG1; lanes 3–7, as in lane 2 but 50, 100, 200, 400, and 800 nM APE1-WT, respectively; lanes 10–14, same as lane 9 but 50, 100, 200, 400, and 800 nM APE1-NΔ61, respectively. After the reaction, all the samples were mildly treated with piperidine (10% [v/v] for 30 min at 37°C) for cleavage at AP sites. Substrate and cleavage product sizes are indicated to the right of the gel. "19*mer" denotes cleavage product containing 3′-terminal α,β-unsaturated phosphoaldehyde and "19mer" means a cleavage product containing a 3′-terminal hydroxyl group. (*B*) Graphical representation of the stimulation of human OGG1-catalyzed DNA glycosylase activity by the APE1 proteins.

Figure 2. Effects of the APE1 proteins on DNA binding and processing by OGG1. (*A*) The OGG1 and APE1 proteins were mixed with the FRET-8oxoG•C duplex oligonucleotide and incubated at 37°C in BER-EDTA buffer. The FRET signal was measured by the stopped-flow technique. In brief, 1.0 μM OGG1 was mixed with a preincubated solution of 1.0 μM APE1-WT and 1.0 μM FRET-8oxoG•C duplex (cyan); 1.0 μM OGG1 was mixed with 1.0 μM FRET-8oxoG•C duplex (black); a preincubated solution of 1.0 μM OGG1 and 1.0 μM APE1-Δ61 was mixed with the FRET-8oxoG•C duplex (blue); a preincubated solution of 1.0 μM OGG1 and 1.0 μM APE1-WT was mixed with the FRET-8oxoG•C duplex (red); 2.0 μM APE1-WT was mixed with 1.0 μM FRET-8oxoG•C duplex (dark yellow); a preincubated

solution of 1.0 μM OGG1 and 1.0 μM Nfo was mixed with the FRET-8oxoG•C duplex (magenta). (*B*) The OGG1 and APE1 proteins were mixed with the FRET-F•C duplex oligonucleotide and incubated at 37°C in BER-EDTA buffer. In brief, 1.0 μM APE1-WT was mixed with 1.0 μM FRET-F•C duplex (black); 1.0 μM OGG1 was mixed with 1.0 μM FRET-F•C duplex (cyan); 1.0 μM APE1-WT was mixed with a preincubated solution of 1.0 μM OGG1 and 1.0 μM FRET-F•C duplex (blue).

Figure 3. Stimulation of human MBD4^{cat}-catalyzed DNA glycosylase activity by the APE1-WT or APE1-NΔ61 proteins. (*A*) Denaturing PAGE analysis of the cleavage products. Briefly, 50 nM 5′-^{32}P-labeled 22mer U•G duplex oligonucleotide was incubated in BER-EDTA reaction buffer for 30 min at 37°C in the presence of 20 nM MBD4^{cat} and various concentrations of APE1-WT or truncated APE1-NΔ61. Lane 1, 50 nM U•G; lane 2, as in lane 1 but 20 nM MBD4^{cat}; lanes 3–6, as in lane 2 but 250, 500, 1000, and 2000 nM APE1-WT; lane 7, 50 nM U•G; lane 8, as in lane 7 but 20 nM MBD4^{cat}; lanes 9–12, as in lane 8 but 250, 500, 1000, and 2000 nM APE1-NΔ61, respectively. After the reaction, all the samples were mildly treated with piperidine (10% [v/v] 30 min at 37°C) for cleavage at AP sites. Substrate and cleavage product sizes are indicated to the right of the gel. "9*mer" denotes a cleavage product containing 3′-terminal α,β-unsaturated phosphoaldehyde, and "9mer" denotes a cleavage product containing a 3′-terminal hydroxyl group. (*B*) Graphical representation of the stimulation of human MBD4^{cat}-catalyzed DNA glycosylase activity on 22- and 63mer U•G substrates by the APE1-WT or APE1-NΔ61 proteins.

Figure 4. Effects of the APE1 proteins on DNA binding and processing by MBD4^{cat}. The MBD4^{cat} and APE1 proteins were mixed with the FRET-U•G duplex oligonucleotide and incubated at 37°C in BER-EDTA buffer. The FRET signal was measured by the stopped-flow

technique. In brief, 2.0 μM MBD4^{cat} was mixed with 1.0 μM FRET-U•G duplex (black); a preincubated solution of 2.0 μM MBD4^{cat} and 1.0 μM APE1-Δ61 was mixed with the FRET-U•G duplex (blue); a preincubated solution of 2.0 μM MBD4^{cat} and 1.0 μM APE1-WT was mixed with the FRET-U•G duplex (red).

Figure 5. **Stimulation of human ANPG^{cat}-catalyzed Hx-DNA glycosylase activity by APE1-WT or APE1-NΔ61**. (*A*) Denaturing PAGE analysis of the cleavage products. In brief, 50 nM 5′-^{32}P-labeled 40mer Hx•T duplex oligonucleotide was incubated in BER-EDTA reaction buffer for 30 min at 37°C in the presence of 15 nM ANPG^{cat} and various concentrations of APE1-WT or truncated APE1-NΔ61. Lanes 1 and 7, 50 nM Hx•T; lanes 2 and 8, as in lane 1 but 1 5 nM ANPG^{cat}; lanes 3–6, as in lane 2 but 250, 500, 1000, and 2000 nM APE1-WT, respectively; lanes 9–12, as in lane 8 but 250, 500, 1000, and 2000 nM APE1-NΔ61, respectively. After the reaction, all the samples were mildly treated with piperidine (10% [v/v], 30 min at 37°C) for cleavage at AP sites. Substrate and cleavage product sizes are indicated to the right of the gel. (*B*) Graphical representation of stimulation of human ANPG^{cat}-catalyzed DNA glycosylase activity by the APE1-WT and APE1-NΔ61 proteins.

Figure 6. **Interactions of the APE1-WT or APE1-NΔ61 proteins with a 1440-bp linear undamaged duplex DNA fragment**. Filtered dark-field electron microscopy images of 5 nM 1440-bp linear dsDNA fragment incubated with 100 nM APE1 in binding buffer (10 mM Tris-HCl pH 8, 50 mM NaCl). (**a1** and **a2**) Control DNA without the protein; (**b1–b3**) Polymerization of APE1-WT on DNA can be observed near DNA ends indicated by arrows; (**c1** and **c2**) APE1-WT oligomers on DNA induce conformational distortions of the DNA helix and intramolecular DNA folding indicated by thin arrows; (**d1** and **d2**) further oligomerization of APE1-WT along DNA fragments promotes intermolecular aggregation *via*

DNA bridging resulting in the formation of networks and DNA compaction marked by thick arrows; (**e1** and **e2**) oligomerization of APE1-NΔ61 on DNA. Only a few DNA conformational changes can be observed without bridging events. Scale bar = 200 nm.

Figure 7. The interaction of the APE1-WT protein with an AP site–containing DNA fragment. A 210-bp linear DNA fragment containing an AP site was incubated with APE1-WT in binding buffer (10 mM Tris-HCl pH 8, 50 mM NaCl). (**a** and **b**) Control DNA without the protein; (**c–f**) Various shapes of the interaction complex of APE1 with the AP site located in the middle of the DNA fragment. APE1 polymerizes along DNA to recognize an AP site and induces a drastic DNA backbone kink. The scale bars are 50 nm. (**g**) Angle measurements of the 210-bp linear DNA fragment containing an AP site. Distribution of the angles induced by the AP site alone or recognized by APE1. The AP site at the center induces curvature of ~30° and the presence of APE1 on this abasic site induces curvature centered around 90°. Calculation of Spearman's rank correlation coefficient showed a significant correlation between angle values obtained with free DNA and with APE1–AP site complexes ($p < 0.0001$).

Figure 8. **APE1-catalyzed cleavage of αdA•T duplex oligonucleotides of various lengths (17- to 64mer)**. In brief, 10 nM 5′-^{32}P-labeled 17-, 22-, 43-, or 64mer αdA•T duplex oligonucleotides were incubated in NIR reaction buffer for 0–60 min at 37°C in the presence of 2 nM APE1-WT. (*A*) Denaturing PAGE analysis of cleavage products of 17mer and 64mer αdA•T duplexes by APE1-WT. Substrate and cleavage product sizes are indicated to the right of the gel. (*B*) Graphical representation of the time-dependent cleavage of αdA•T duplexes by APE1-WT.

Figure 9. **Graphical representation of time-dependent cleavage of THF•T and αdA•T duplexes by APE1-NΔ61 or *E. coli* Nfo**. In brief, 10 nM 5′-^{32}P-labeled 17-, 22-, 43-, and 64mer THF•T or αdA•T duplex oligonucleotides were incubated in respective buffers for 0–10 min at 37°C in the presence of 0.5 nM APE1-NΔ61 or 0.1 nM Nfo. (*A*) Time-dependent cleavage of THF•T duplexes by APE1-NΔ61. (*B*) Time-dependent cleavage of αdA•T duplexes by *E. coli* Nfo.

Figure 10. **The putative mechanism of the APE1-catalyzed stimulation of DNA glycosylases and redox activity**. (1) APE1 binds to transient single-stranded structures present at the termini of duplex DNA. (2) Multiple molecules of APE1 polymerize on the DNA fragment and form oligomerlike complexes. (3) APE1 oligomers on DNA induce conformational changes in the DNA helix, and this change stimulates DNA glycosylase activities and sequence-specific binding of transcription factors to DNA.

FIGURES

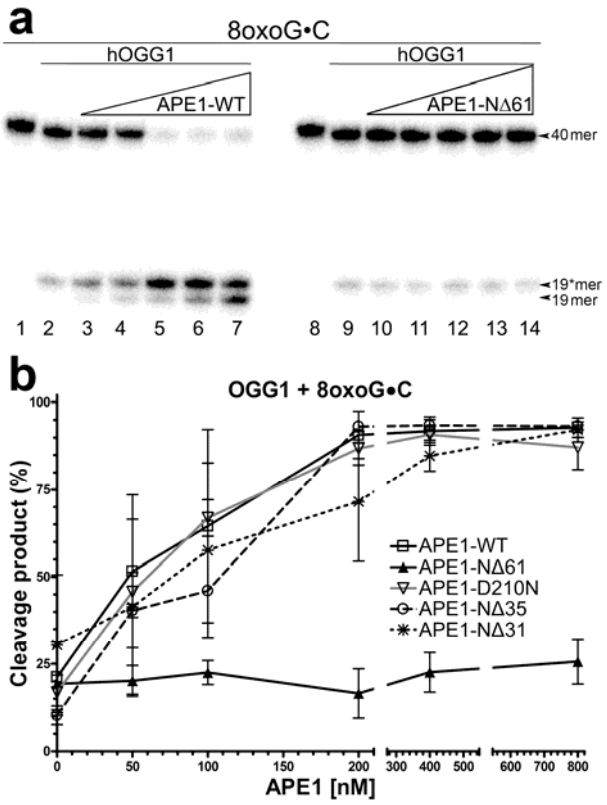

Figure 1

A

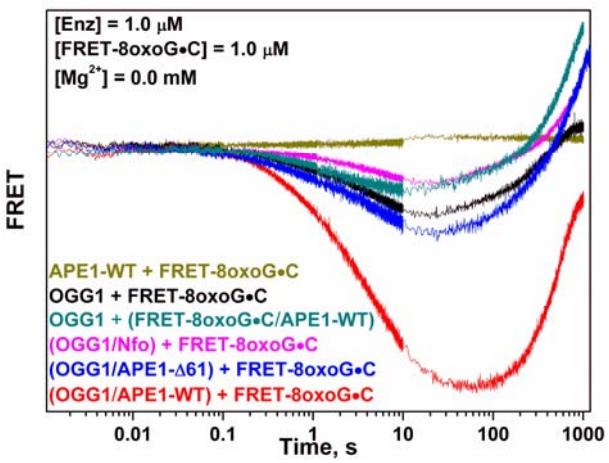
[Enz] = 1.0 μM
[FRET-8oxoG•C] = 1.0 μM
[Mg2+] = 0.0 mM
FRET
APE1-WT + FRET-8oxoG•C
OGG1 + FRET-8oxoG•C
OGG1 + (FRET-8oxoG•C/APE1-WT)
(OGG1/Nfo) + FRET-8oxoG•C
(OGG1/APE1-Δ61) + FRET-8oxoG•C
(OGG1/APE1-WT) + FRET-8oxoG•C
0.01
0.1
1
10
100
1000
Time, s

B

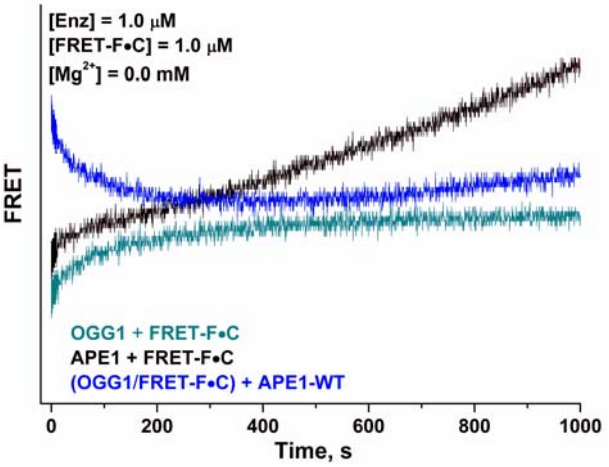
[Enz] = 1.0 μM
[FRET-F•C] = 1.0 μM
[Mg2+] = 0.0 mM
FRET
OGG1 + FRET-F•C
APE1 + FRET-F•C
(OGG1/FRET-F•C) + APE1-WT
0
200
400
600
800
1000
Time, s

Figure 2

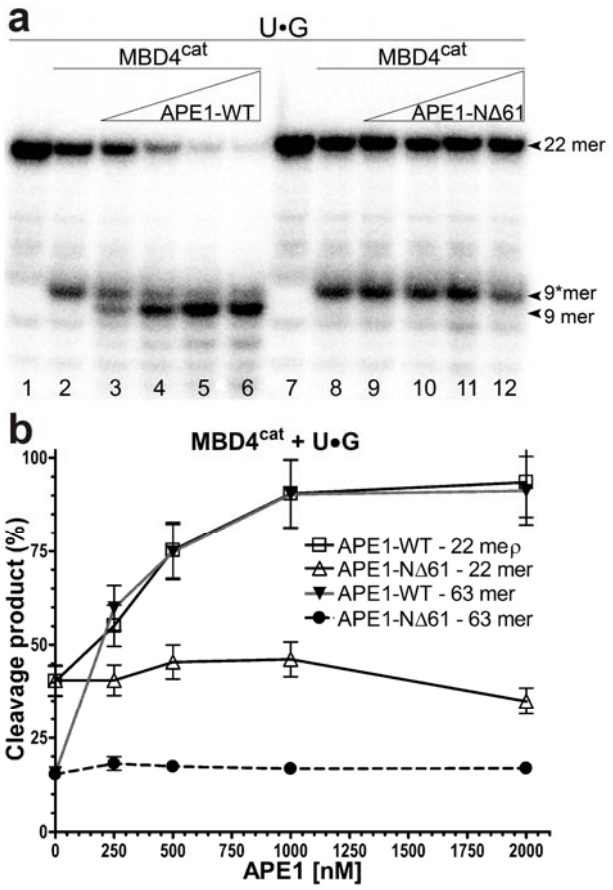
a
U•G
MBD4cat
APE1-WT
MBD4cat
APE1-NΔ61
22 mer
9*mer
9 mer
1 2 3 4 5 6 7 8 9 10 11 12
b
MBD4cat + U•G
Cleavage product (%)
100
75
50
25
0
APE1-WT - 22 meρ
APE1-NΔ61 - 22 mer
APE1-WT - 63 mer
APE1-NΔ61 - 63 mer
0 250 500 750 1000 1250 1500 1750 2000
APE1 [nM]

Figure 3

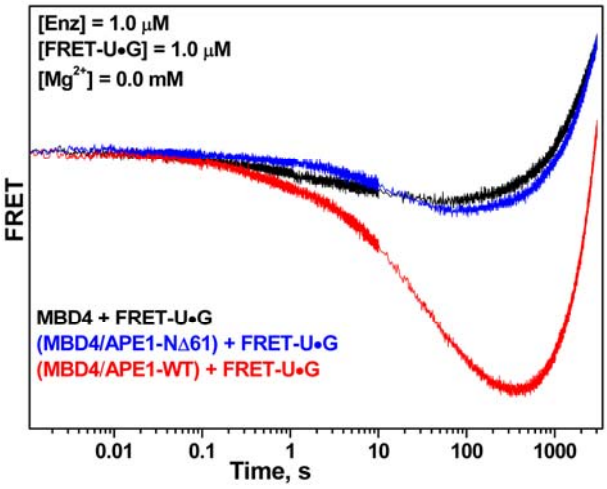
[Enz] = 1.0 μM
[FRET-U•G] = 1.0 μM
[Mg2+] = 0.0 mM
FRET
MBD4 + FRET-U•G
(MBD4/APE1-NΔ61) + FRET-U•G
(MBD4/APE1-WT) + FRET-U•G
0.01
0.1
1
10
100
1000
Time, s

Figure 4

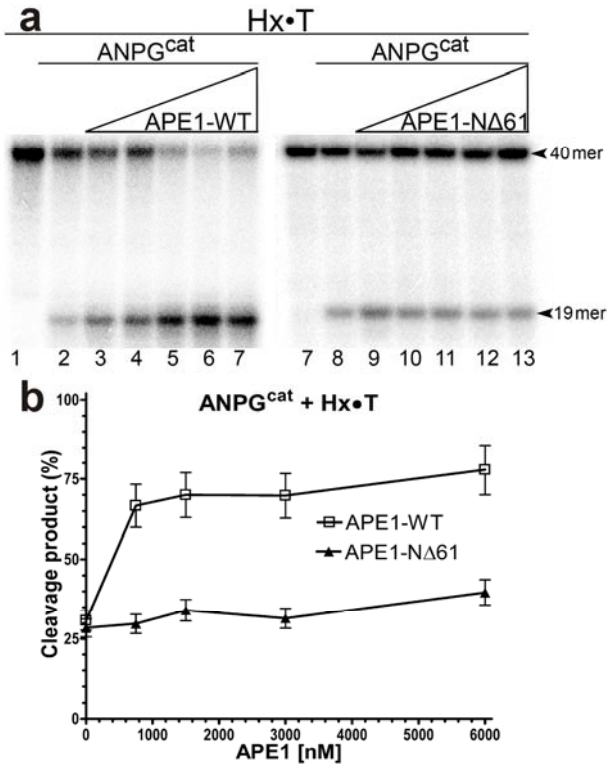
a
Hx•T
ANPG^cat
APE1-WT
ANPG^cat
APE1-NΔ61
40mer
19mer
1 2 3 4 5 6 7 7 8 9 10 11 12 13
b
ANPG^cat + Hx•T
Cleavage product (%)
APE1-WT
APE1-NΔ61
APE1 [nM]

Figure 5

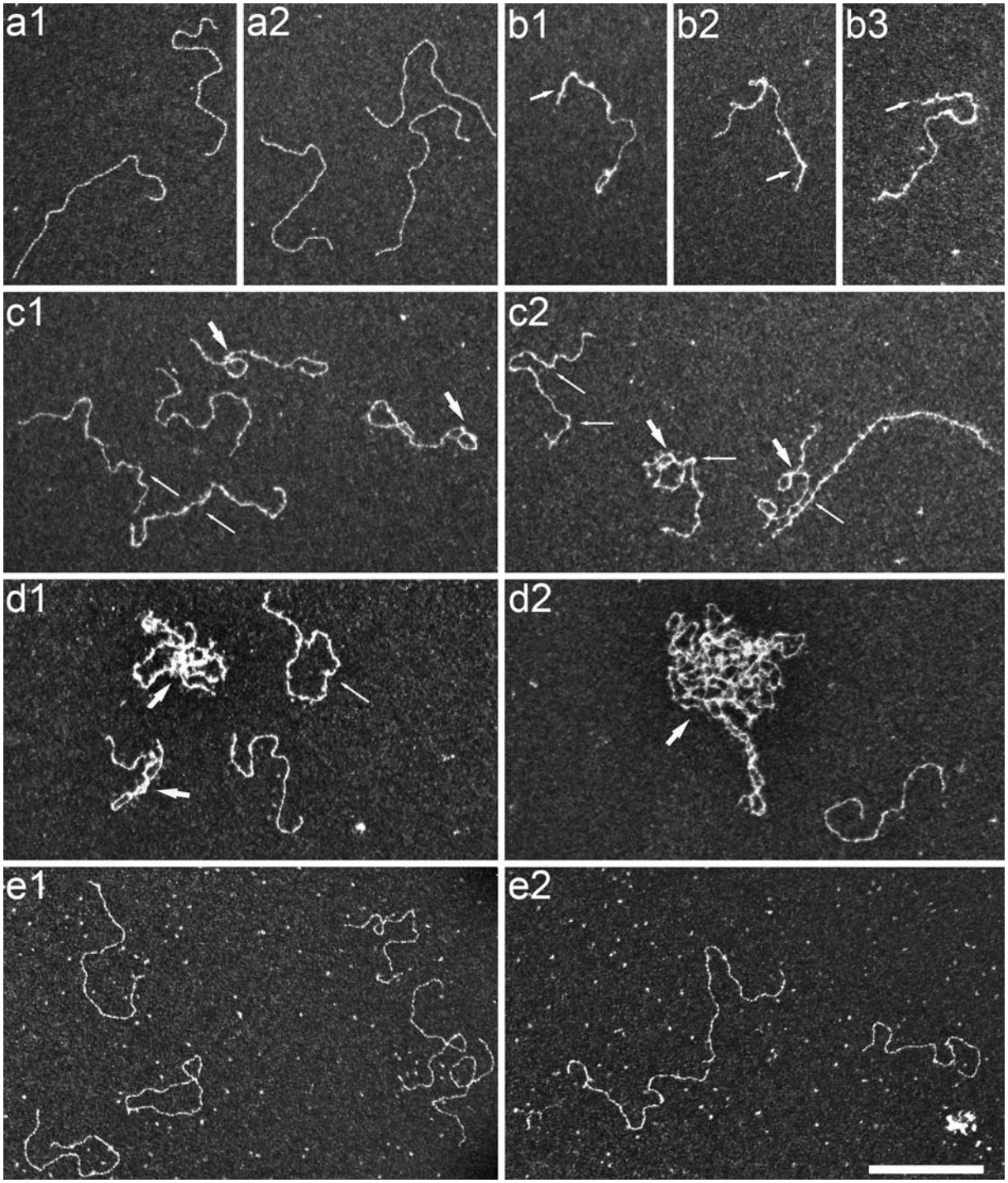

Figure 6

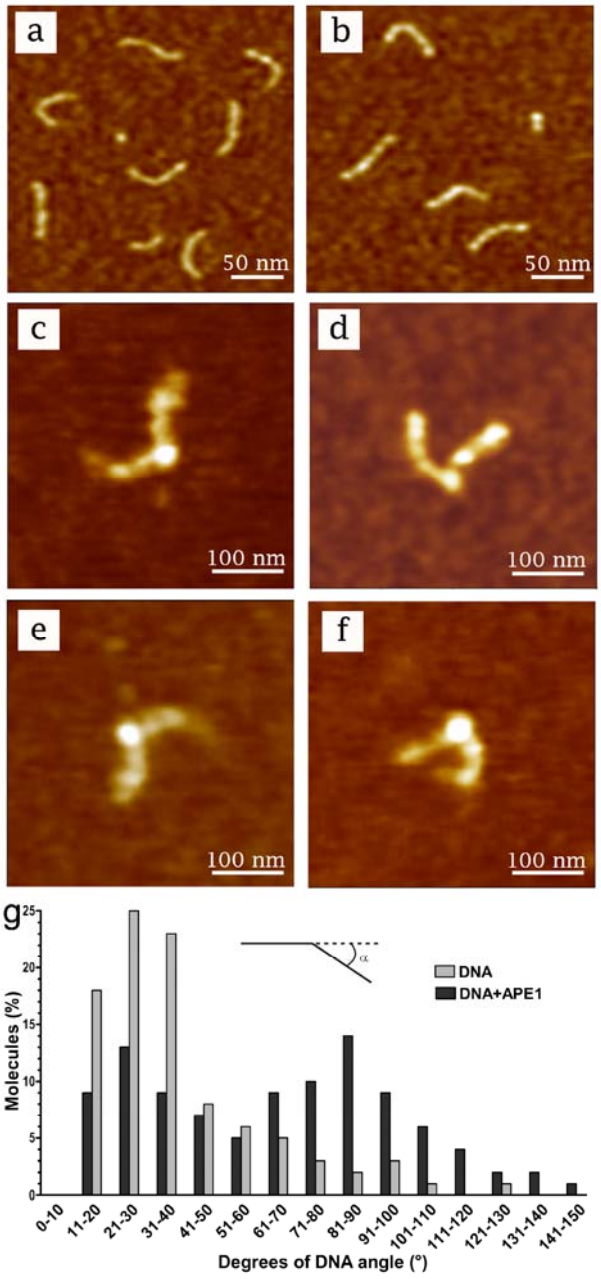
a
50 nm
b
50 nm
c
100 nm
d
100 nm
e
100 nm
f
100 nm
g
Molecules (%)
0
5
10
15
20
25
α
DNA
DNA+APE1
0-10
11-20
21-30
31-40
41-50
51-60
61-70
71-80
81-90
91-100
101-110
111-120
121-130
131-140
141-150
Degrees of DNA angle (°)

Figure 7

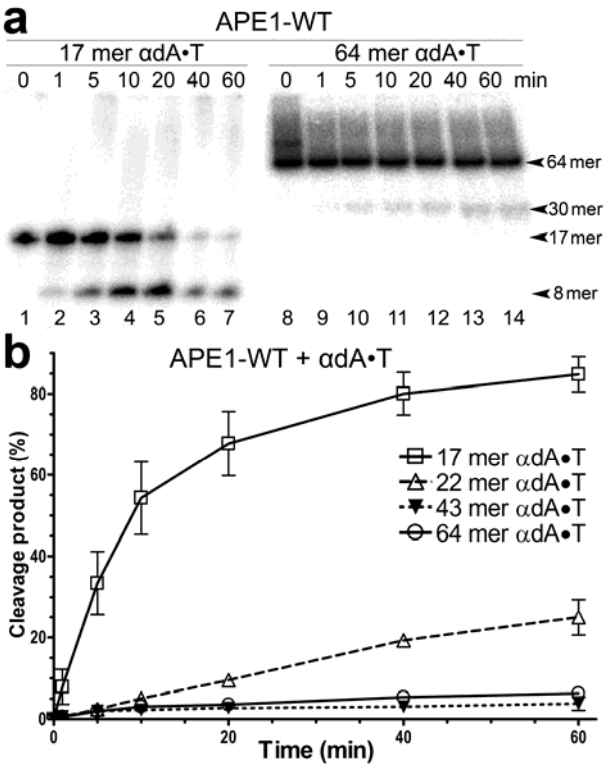
a
APE1-WT
17 mer αdA•T
64 mer αdA•T
0 1 5 10 20 40 60
0 1 5 10 20 40 60 min
64 mer
30 mer
17 mer
8 mer
1 2 3 4 5 6 7
8 9 10 11 12 13 14
b
APE1-WT + αdA•T
Cleavage product (%)
Time (min)
17 mer αdA•T
22 mer αdA•T
43 mer αdA•T
64 mer αdA•T

Figure 8

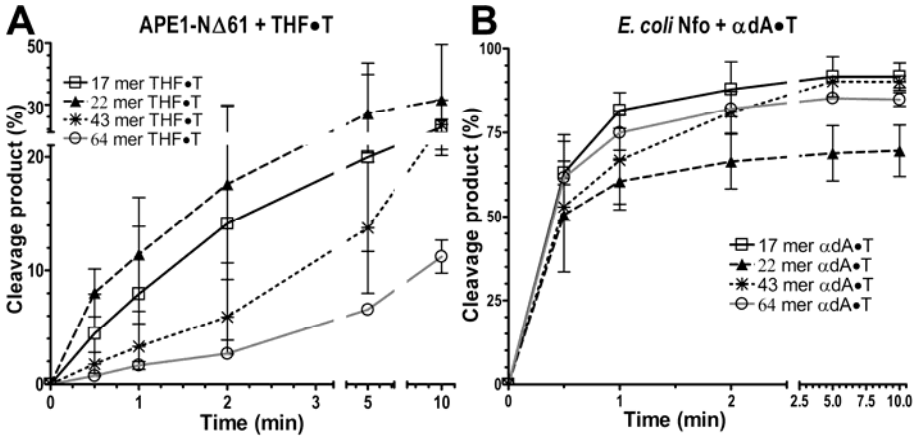
A
APE1-NΔ61 + THF•T
17 mer THF•T
22 mer THF•T
43 mer THF•T
64 mer THF•T
Cleavage product (%)
Time (min)
B
E. coli Nfo + αdA•T
17 mer αdA•T
22 mer αdA•T
43 mer αdA•T
64 mer αdA•T
Cleavage product (%)
Time (min)

Figure 9

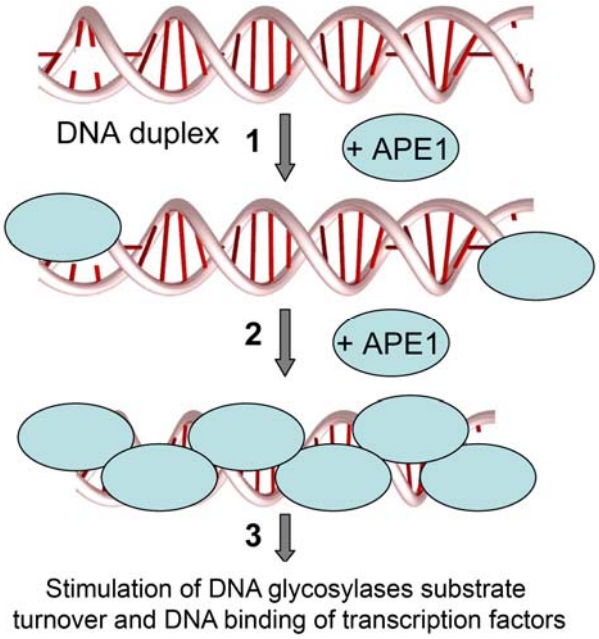
DNA duplex
1
+ APE1
2
+ APE1
3
Stimulation of DNA glycosylases substrate
turnover and DNA binding of transcription factors

Figure 10

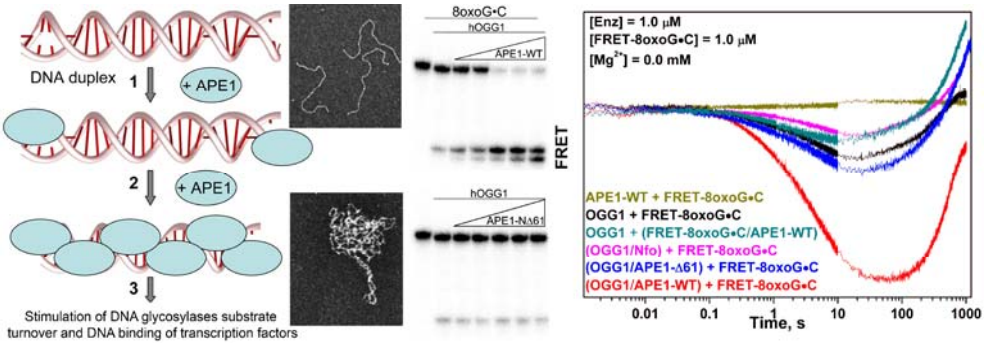
DNA duplex
1
+ APE1
2
+ APE1
3
Stimulation of DNA glycosylases substrate turnover and DNA binding of transcription factors
8oxoG•C
hOGG1
APE1-WT
hOGG1
APE1-NΔ61
FRET
[Enz] = 1.0 μM
[FRET-8oxoG•C] = 1.0 μM
[Mg2+] = 0.0 mM
APE1-WT + FRET-8oxoG•C
OGG1 + FRET-8oxoG•C
OGG1 + (FRET-8oxoG•C/APE1-WT)
(OGG1/Nfo) + FRET-8oxoG•C
(OGG1/APE1-Δ61) + FRET-8oxoG•C
(OGG1/APE1-WT) + FRET-8oxoG•C
0.01
0.1
1
10
100
1000
Time, s

TOC

Supporting Information

The role of the N-terminal domain of human apurinic/apyrimidinic endonuclease 1, APE1, in DNA glycosylase stimulation

Olga Kladova[a], Milena Bazlekowa-Karaban[b,c], Sonia Baconnais[d], Olivier Pietrement[d], Alexander A. Ishchenko[c], Bakhyt T. Matkarimov[e], Danila A. Iakovlev[a], Andrey Vasenko[f], Olga S. Fedorova[a], Eric Le Cam[d], Barbara Tudek[b,g], Nikita A. Kuznetsov[a,] And Murat Saparbaev[c,]**

[a]*SB RAS Institute of Chemical Biology and Fundamental Medicine, Novosibirsk 630090, Russia.*
[b]*Institute of Biochemistry and Biophysics, Polish Academy of Sciences, 02-106 Warsaw, Poland.*
[c]*Groupe «Réparation de l'ADN», Equipe Labellisée par la Ligue Nationale contre le Cancer, CNRS UMR8200, Université Paris-Sud, Gustave Roussy Cancer Campus, F-94805 Villejuif Cedex, France.*
[d]*CNRS UMR8126, Université Paris-Sud, Gustave Roussy Cancer Campus, F-94805 Villejuif Cedex, France.*
[e]*National laboratory Astana, Nazarbayev University, Astana 010000, Kazakhstan.*
[f]*National Research University Higher School of Economics, 101000 Moscow, Russia*
[g]*Institute of Genetics and Biotechnology, University of Warsaw, Warsaw, Poland.*

Table S1. Linear velocities of the cleavage of αdA•T and THF•T oligonucleotide duplexes of varying length by Nfo, APE1 and APE1-NΔ61.

Enzyme	DNA substrate			
	17 mer αdA•T	22 mer αdA•T	43 mer αdA•T	64 mer αdA•T
Nfo	9.045 ± 1.259[a]	6.860 ± 1.149	7.459 ± 1.107	8.459 ± 1.368
APE1 WT	0.181 ± 0.032	0.044 ± 0.0013	0.0076 ± 0.0014	0.0123 ± 0.0015
	DNA substrate			
	17 mer THF•T	22 mer THF•T	43 mer THF•T	64 mer THF•T
Nfo	7.787 ± 1.709[a]	9.662 ± 2.128	6.055 ± 1.198	8.764 ± 1.928
APE1 WT	0.644 ± 0.0998	0.357 ± 0.005	0.155 ± 0.0071	0.106 ± 0.023
APE1-NΔ61	0.281 ± 0.051	0.385 ± 0.068	0.245 ± 0.009	0.117 ± 0.004

[a]Linear velocities are given in nM/min.

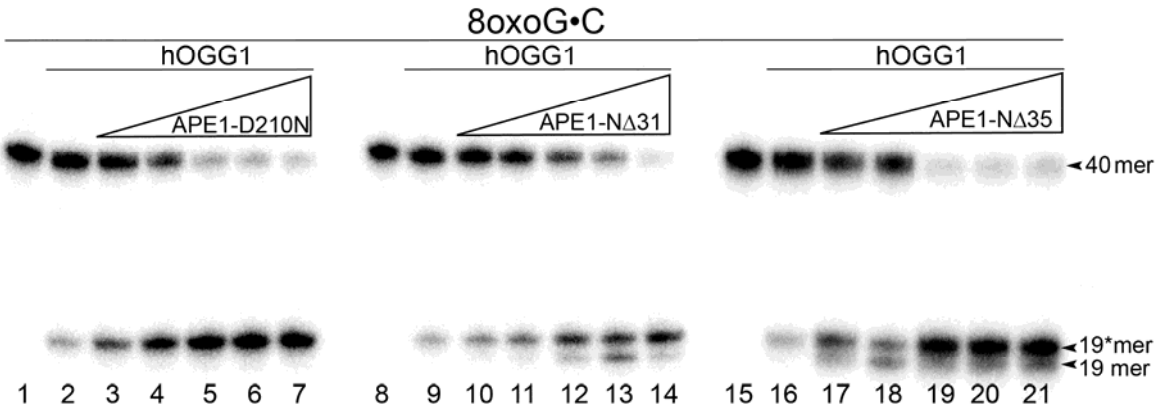

Supplementary Figure S1. **Stimulation of human OGG1-catalyzed DNA glycosylase activity by APE1-D210N and truncated APE1-NΔ31 and APE1-NΔ35 proteins**. In brief, 50 nM 5'-^{32}P-labeled 40mer 8oxoG•C duplex oligonucleotide was incubated in BER-EDTA reaction buffer for 30 min at 37°C in the presence of 15 nM OGG1 and varying concentrations of APE1-D210N, APE1-NΔ31 or APE1-NΔ35. Lanes 1, 8 and 15, 50 nM 8oxoG•C; lanes 2, 9 and 16, as in lane 1 but 15 nM OGG1; lanes 3–7, as in lane 2 but 50, 100, 200, 400, and 800 nM APE1-D210N, respectively; lanes 10–14, same as lane 9 but 50, 100, 200, 400, and 800 nM APE1-NΔ31, respectively; lanes 17–21, as in lane 16 but 50, 100, 200, 400, and 800 nM APE1-NΔ35, respectively. After the reaction, all the samples were treated with light piperidine (10% [v/v], 30 min at 37°C) for cleavage at AP sites. Substrate and cleavage product sizes are indicated to the right of the gel. "19*mer" denotes cleavage product containing 3'-terminal α,β-unsaturated phosphoaldehyde and "19mer" denotes cleavage product containing 3'-terminal hydroxyl group.

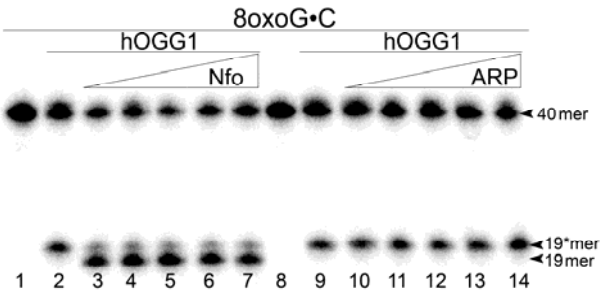

Supplementary Figure S2. **Stimulation of human OGG1-catalyzed DNA glycosylase activity by bacterial and plant AP endonucleases**. Briefly, 50 nM 5'-^{32}P-labeled 40mer 8oxoG•C duplex oligonucleotide was incubated in BER-EDTA reaction buffer for 30 min at 37°C in the presence of 15 nM OGG1 and varying concentrations of *E. coli* Nfo or *A. thaliana* ARP. Lanes 1 and 8, 50 nM 8oxoG•C; lanes 2 and 9, as in lane 1 but 15 nM OGG1; lanes 3–7, as in lane 2 but 50, 100, 200, 400, and 800 nM Nfo, respectively; lanes 10–14, same as lane 9 but 50, 100, 200, 400, and 800 nM ARP, respectively. After the reaction, all the samples were treated with light piperidine (10% [v/v], 30 min at 37°C) for cleavage at AP sites. Substrate and cleavage product sizes are indicated to the right of the gel. "19*mer" denotes cleavage product containing 3'-terminal α,β-unsaturated phosphoaldehyde and "19mer" denotes cleavage product containing 3'-terminal hydroxyl group.

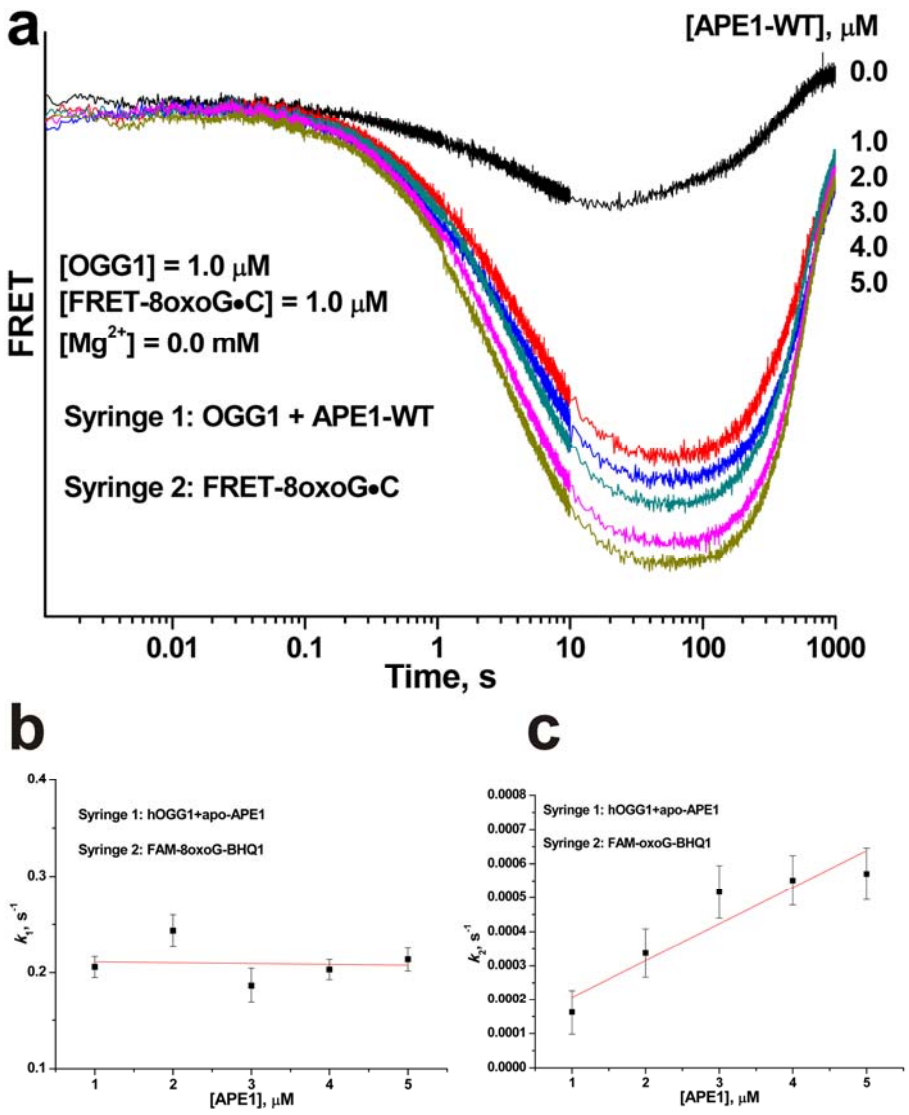

Supplementary Figure S3. Effect of APE1-WT on DNA binding and catalysis of OGG1. (**a**) The OGG1 and APE1-WT proteins were mixed with the FRET-8oxoG•C duplex oligonucleotide and incubated at 37°C in BER-EDTA buffer. The FRET signal was measured by the stopped-flow technique. In brief, 1.0 μM OGG1 was incubated with various concentrations (indicated right to the kinetic traces) of APE1-WT and then mixed with 1.0 μM FRET-8oxoG•C duplex. Dependence of the observed rate constants k_1 (**b**) and k_2 (**c**) on APE1-WT concentration.

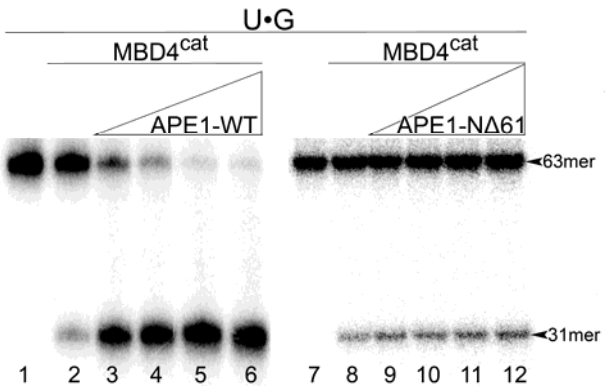

Supplementary Figure S4. **Stimulation of human MBD4^{cat} on the 63mer U•G duplex by APE1-WT or APE1-NΔ61**. Denaturing PAGE analysis of the cleavage products. In brief, 50 nM 5'-^{32}P-labeled 63mer U•G duplex oligonucleotide was incubated in BER-EDTA reaction buffer for 30 min at 37°C in the presence of 20 nM MBD4^{cat} and varying concentrations of APE1-WT and APE1-NΔ61. Lanes 1 and 7, 50 nM 63mer U•G; lanes 2 and 8, as in lane 1 but 20 nM MBD4^{cat}; lanes 3–6, as in lane 2 but 250, 500, 1000, and 2000 nM APE1-WT; lane 7, 50 nM U•G; lane 8, as in lane 7 but 20 nM MBD4^{cat}; lanes 9–12, as in lane 8 but 250, 500, 1000, and 2000 nM APE1-NΔ61. After the reaction, all the samples were treated with light piperidine (10% [v/v], 30 min at 37°C) for cleavage at AP sites. Substrate and cleavage product sizes are indicated to the right of the gel.

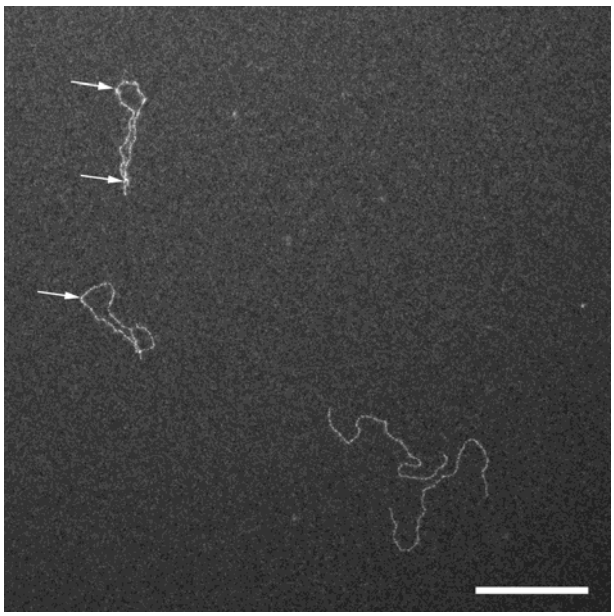

Supplementary Figure S5. **Interactions of the APE1-WT protein with a 1440-bp linear undamaged duplex DNA fragment**. Filtered dark-field electron microscopy images of 5 nM 1440-bp linear dsDNA fragment incubated with 100 nM APE1 in binding buffer (10 mM Tris-HCl pH 8, 50 mM NaCl) for 10 min at 4°C. Scale bar = 200 nm.

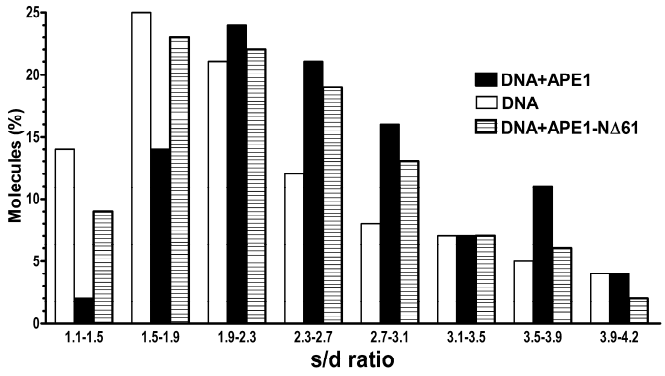

Supplementary Figure S6. Histogram of number of complexes (percentage) according to the s/d ratio. The s/d is the ratio between DNA contour length and end to end distances of 1440-bp DNA fragment in the presence or absence of APE1 and APE1-NΔ61. The percentage of analyzed molecules is reported on the Y-axis; n=120 for each condition. The Spearman's rank correlation coefficient between the s/d ratios in the presence of APE1-WT show significant correlation $p<0,001$ and no correlation between the s/d ratios in the presence of APE1-NΔ61 mutant.

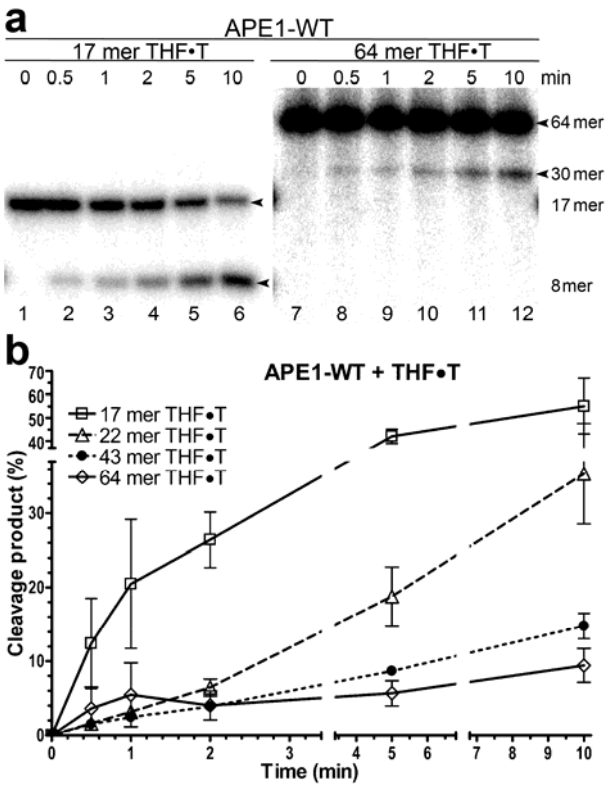

Supplementary Figure S7. **APE1-catalyzed cleavage of AP site containing duplex oligonucleotides of varying lengths (17-64 bp)**. (**a**) Denaturing PAGE analysis of cleavage products. 10 nM 5'-^{32}P-labelled 17 and 64 mer THF•T duplex oligonucleotides were incubated in the BER reaction buffer for 0-10 min at 37°C in the presence of 0.1 nM APE1-WT. Substrate and cleavage product sizes are indicated to the right of the gel. For details see Materials and Methods. (**b**) Graphical representation of time-dependent cleavage of THF•T duplexes by APE1-WT.

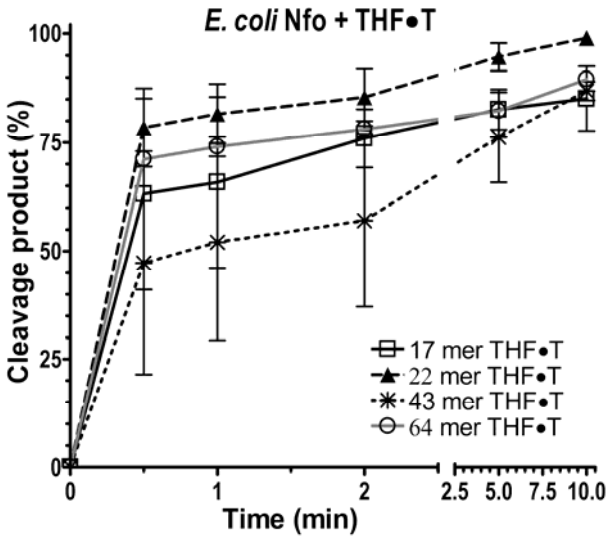

Supplementary Figure S8. **Graphical representation of time-dependent cleavage of THF•T duplexes by *E. coli* Nfo**. Briefly, 10 nM 5'-^{32}P-labeled 17-, 22-, 43-, or 64mer THF•T duplex oligonucleotides were incubated in Nfo buffer for 0–10 min at 37°C in the presence of 0.1 nM Nfo.

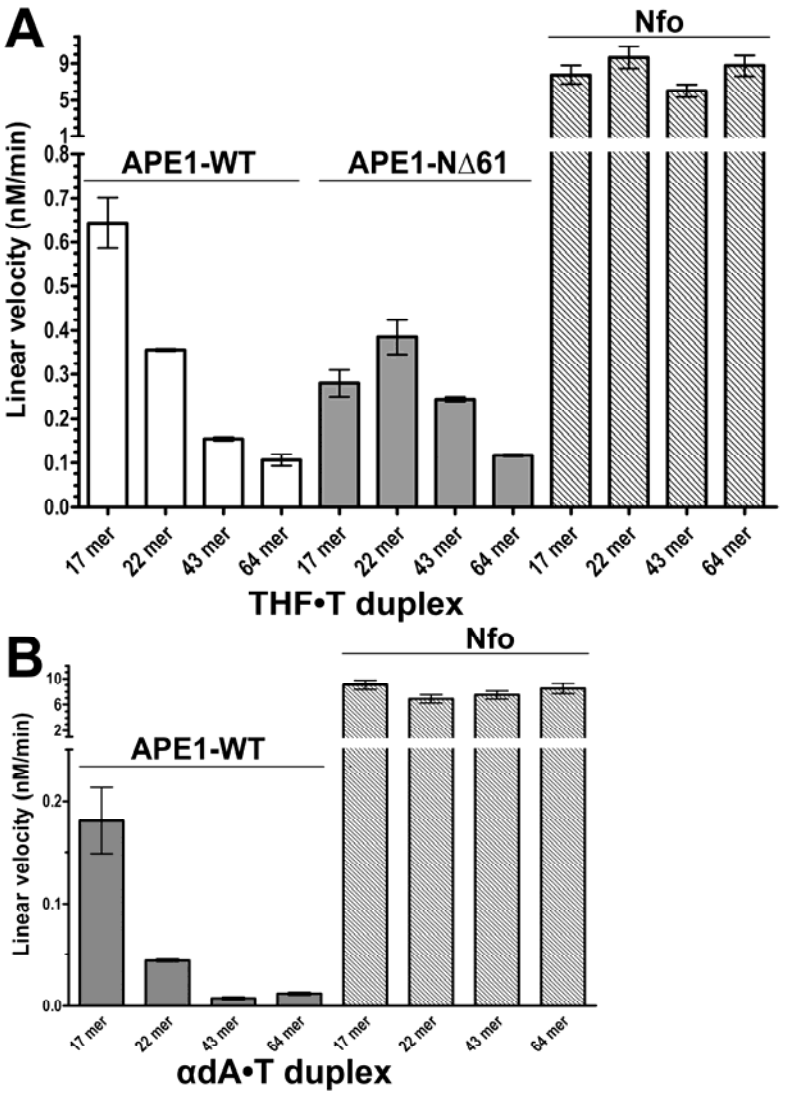

Supplementary Figure S9. Histogram of linear velocities of the cleavage of THF•T (A) and αdA•T (B) oligonucleotide duplexes of varying length by Nfo, APE1 and APE1-NΔ61.